INTERNATIONAL ATOMIC ENERGY AGENCY
UNITED NATIONS EDUCATIONAL, SCIENTIFIC AND CULTURAL ORGANIZATION
INTERNATIONAL CENTRE FOR THEORETICAL PHYSICS
I.C.T.P., P.O. BOX 586, 34100 TRIESTE, ITALY, CABLE CENTRATOM TRIESTE

H4.SMR/449-4

**WINTER COLLEGE ON**
**HIGH RESOLUTION SPECTROSCOPY**

**(8 January - 2 February 1990)**

# INSTABILITIES AND SPATIAL COMPLEXITY IN A LASER

L. A. LUGIATO,

(**) G.-L. OPPO, J.R. TREDICCE & L.M. NARDUCCI

**Dipartimento di Fisica del Politecnico**
**10129 Torino, Italy**

**(**) Physics Department, Drexel University**
**Philadelphia, PA 19104, U.S.A.**

# Instabilities and spatial complexity in a laser

**L.A. Lugiato**
Dipartimento di Fisica, Politecnico di Torino, 10129 Torino, Italy

**G.L. Oppo, J.R. Tredicce and L.M. Narducci**
Physics Department, Drexel University, Philadelphia, Pa. 19104

**Abstract**

We discuss the emergence of spatial structures in a ring laser model with transverse effects. The emphasis of this work is with the development of a description that can capture the essential features of transverse dynamics without the need for large-scale numerical efforts. We introduce an extension of the uniform field limit and derive a set of modal equations which we solve with conventional numerical methods. Our solutions show evidence of transverse mode competition in the laser dynamics leading to both time-dependent and multi-mode stationary (cooperative frequency locking) behaviors. In the time-dependent regime we analyze the resulting spatial structures and suggest a scheme for the investigation and characterization of spatial complexity.



## 1. Introduction

The governing principles that control the transition from disordered to ordered states and from order to complexity have been the focus of active investigations during the last twenty years. Recent advances have clarified some of the mechanisms by which spatial structures emerge from an initially homogeneous state with a break of space-translational symmetry, and have shown how a system with time-independent parameters can develop oscillatory patterns and break the original time-translational symmetry.[1] In addition, it is now well established that even system described by a small number of ordinary differential equations can produce complex temporal patterns, such as quasi periodicity, period doubling and chaos;[2] these phenomena are characterized by simple scaling laws that apply uniformly to large classes of nonlinear dynamical systems.[3] Important milestones in the optical domain have been reached with the experimental observation and characterization of chaos in both passive[4] and active[5,6] optical systems

Special techniques, developed for the study of the fractal nature of strange attractors, have provided useful tools for the identification of dynamical chaos and diagnostic tests to characterize the chaotic behaviors of both computer simulations and experimental data.[7,8] Furthermore, these methods have established links with the current theories of fractals which are one of the main avenues for understanding the appearance of complexity from simple iterative procedures.

Even if sometimes chaotic behavior has been labelled as turbulent, we now recognize that the investigation of turbulent phenomena and spatio-temporal complexity requires consideration of both space and time evolution.[9] Much of the recent research on the dynamics of nonlinear optical systems has dealt with on the temporal behavior in the plane-wave approximation for the electric field. Transverse effects, however, have begun to attract growing interest especially in passive systems without population inversion. Intense radiation in a strongly absorbing medium can undergo self focusing and produce spatial ring structures.[10] Modulational instabilities modify the transverse profile and produce period doubling and chaos.[11] Arrays of bistable systems can display patterns with remarkable spatial complexity.[12] An example of formation of stationary transverse structures from a homogeneous configuration with spontaneous breaking of the

translational symmetry was demonstrated with the help of a simple analytic model;[13] the same type of instability is responsible for the emergence of spatial soliton patterns on top of a broad Gaussian profile.[14] The spontaneous breaking of the cylindrical symmetry has been discovered numerically,[15] described analytically,[16] and observed experimentally.[17,18]

Very recent studies have looked into the problem of spatial pattern formation in laser systems, which is also the main subject of this contribution. Typically, these phenomena are associated with a process called cooperative frequency locking;[19,20] this is a mode of operation of the laser for which supporting experimental evidence was provided in references 21,22. Our aim is to develop a convenient mathematical framework for the study of transverse effects in a unidirectional ring laser with a suitable generalization of the traditional Maxwell-Bloch equations for a collection of homogeneously broadened two-level systems, an approach that is well suited to describe propagation and diffraction effects within the slowly varying envelope and paraxial approximations. We assume that the laser operates as a unidirectional ring resonator capable of supporting Gauss-Laguerre modes; these may or may not have cylindrical symmetry, depending upon the operating conditions and the geometrical parameters of the device, as summarized in an extensive appendix (Appendix A). The model includes phenomenological diffraction losses to account for the experimental fact that different transverse field configurations escape at different rates from the partially transmitting output couplers.

Our strategy is based on the derivation of appropriate modal equations for the field and the atomic amplitudes which are consistent with the field boundary conditions and allow the possibility that the pump profile may not be uniform in the transverse direction. We solve the time-dependent modal equations for a variety of geometrical configurations and operating conditions and analyze the transient and steady state behavior especially as we vary the frequency separation between the transverse cavity modes. For the sake of simplicity with the numerical work, we develop a suitable extension of the traditional uniform field limit which, in the framework of the plane-wave theory, has already played a very useful role in uncovering important dynamical features of the laser.[23] Here also, the uniform field limit requires that both the mirror transmittivity and the gain



per pass of the active medium be very small, while their ratio may be arbitrary but finite.

In an earlier study[24] we considered situations where the transverse mode frequency spacing was comparable to the longitudinal free spectral range and proved that, in this case, single-mode steady state operation is possible. Now we are more interested in situations that favor a strong dynamical coupling among the cavity modes and the development of space-time effects that have no counterpart in the traditional plane-wave theory. The strong coupling emerges when the transverse modes have a frequency spacing which is comparable with the cavity linewidth. This situation can be realized, for example, in a cavity with quasi-planar mirrors, where transverse modes with the same value of the longitudinal index may have arbitrarily small frequency spacing, or in quasi confocal cavities, where transverse modes with different values of the longitudinal index may be arranged to be quasi degenerate in frequency. In such instances the close proximity of the transverse modes favors strong interaction and competition and can yield a variety of spatial and spatio-temporal phenomena such as, for example, cooperative frequency locking, mode beating, quasi-periodic and chaotic oscillations.

Our model predicts the appearance of low threshold instabilities, as already noted in Ref. 24, but also predicts the possibility that several transverse modes with different empty cavity resonances may develop synchronous oscillations. This phenomenon, which we call cooperative frequency locking, is especially interesting because the excited cavity modes, as a result of their mutual nonlinear coupling, seek a common operating frequency and lock onto it. Thus the output of the laser in this phase and frequency locked regime eventually acquires a stationary configuration, usually with a rather complex transverse intensity profile.

A closely related phenomenon is the breaking of the spatial symmetry.[16] Resonators with spherical mirrors can support frequency-degenerate modes with different transverse shapes and,normally, different threshold values for laser action. Typically the spatial configuration with the smallest modal volume has the lowest threshold gain and it becomes excited first. When the gain exceeds a certain critical value, additional degenerate modes become unstable and the transverse intensity profile of the laser breaks away from the original symmetry. At the same time,

because of the degenerate nature of the excited modes, no beat patterns can develop, so that the laser undergoes a p- -e spatial symmetry breaking without temporal modulation.

Some early contributions[25-28] have recently been brought to our attention in which the concept of frequency locking was introduced along similar lines as developed in earlier papers of ours[19-21] without knowledge of this prior discoveries. These papers provided both theoretical[25-27] and experimental[28] results related to this phenomenon. Also relevant to this subject are references 29-31. The occurrence of quasi-periodicity and chaos in multitransverse mode regimes was predicted in Ref. 32 and observed experimentally in references 33-35.

This paper is organized as follows. Section 2 describes the basic equations that govern the space-time evolution of this model. Section 3 contains an overview of the steady state solutions and of the most interesting time dependent features; here we also discuss the status of our current studies of the spatial correlation properties of the output intensity. In Section 4 we discuss some additional details of the cooperative frequency locking phenomenon. Finally, in Section 5 we present a summary of our results and discuss some of the open problems that we hope to address in future studies. Appendix A contains some detailed information on the modal structure of a ring resonator which may be useful as a supplement to the derivation of the basic equations of this model. The remaining two appendices give technical details on the derivation of the mode mode coupling coefficients and the two-mode steady state solution.

## 2. Description of the model and derivation of the equations of motion

The theoretical development described in this section is a generalization of the traditional plane-wave model and it includes (i) the effects of diffraction due to the finite cross section of the field and its transverse variations of amplitude and phase, (ii) the wave-front curvature caused by the spherical reflectors, and (iii) the transverse gain variation of the active medium. The atoms, as shown schematically in Fig. 1, are confined within a region of length $L_A$ between the spherical mirrors and are modelled as a collection of homogeneously broadened two-level systems with a transition frequency $\omega_A$, a spectral width $\gamma_\perp$ and a relaxation rate $\gamma_\parallel$ for the population inversion.



The system is governed by the generalized set of Maxwell-Bloch equations

$$-\frac{i}{4}\nabla_\perp^2 F + \frac{\partial F}{\partial \eta} + \frac{1}{v}\frac{\partial F}{\partial \tau} = i\frac{\delta\Omega'}{v}F - \alpha\Lambda P \qquad (2.1a)$$

$$\frac{\partial P}{\partial \tau} = -\left(FD + (1+i\Delta')P\right) \qquad (2.1b)$$

$$\frac{\partial D}{\partial \tau} = -\gamma\left\{-\frac{1}{2}(F^*P + FP^*) + D - \chi\right\} \qquad (2.1c)$$

or the slowly varying envelopes of the field (F) and of the polarization (P), and for the difference etween the excited and ground state population. The field and atomic variables depend on the caled coordinates

$$\eta = \frac{z}{\Lambda}, \qquad \rho = \sqrt{\frac{\pi}{\Lambda\lambda}}\,r, \qquad \tau = \gamma_\perp t, \qquad (2.2)$$

n addition to the polar angle variable $\varphi$. The scaled phase velocity v is defined by

$$v = \frac{c}{\Lambda\gamma_\perp}$$

ollowing the usual practice, the field envelope F is related to the full Maxwell field E by

$$E(r,\varphi,z,t) = \frac{\hbar\sqrt{\gamma_\perp\gamma_\parallel}}{2\mu}\frac{1}{2}\left\{F(r,\varphi,z,t)\exp[i(k_0 z - \omega_0 t)]\exp(-i\delta\Omega t) + c.c.\right\} \qquad (2.3)$$

here $\mu$ denotes the modulus of the dipole moment of the atomic transition. The carrier frequency $\omega_0$ is arbitrary but it must be sufficiently close to the (unknown) operating laser frequency so that F indeed slowly varying in time; a convenient choice for $\omega_0$ is given by the empty cavity sonance, $\omega_{N,0,0}$, that lies nearest to the center of the gain line ($\omega_A$); $k_0 = \omega_0/c = \omega_{N,0,0}/c$ is the orresponding wave number.

In the traditional Maxwell-Bloch theory $\delta\Omega$ denotes the frequency offset between the perating laser frequency and $\omega_0$, under conditions of stationary output intensity; this identification nplies that in steady state F becomes independent of time. Implicit in this representation of the laxwell field is the assumption that $\delta\Omega$ can be calculated in closed form, and this is indeed the ase for single-mode operation in the plane wave-model[23] and for the conditions considered in

Ref. 24. Here, instead, the steady state configuration is often of the multimode type and $\delta\Omega$ cannot be calculated so easily in closed form; for now, we leave this frequency shift unspecified and reserve the right to fix it in the most convenient way when needed in the following calculations. Naturally, for any choice of $\delta\Omega$ other than the correct frequency offset, the steady state values of the derivatives of the field and polarization variables do not vanish; however, any judicious choice of $\delta\Omega$ will make the temporal variations of F slow, and this is advantageous for the purpose of numerical computations.

The remaining symbols that appear in Eqs. (2.1) are defined as follows: $\delta\Omega'$ denotes $\delta\Omega/\gamma_\perp$, $\Delta'$ is the difference between $\delta'_{AC} \equiv (\omega_A - \omega_0)/\gamma_\perp$ and $\delta\Omega'$; $\alpha$ is the unsaturated gain parameter of the field per unit length, and $\chi$ is the equilibrium population difference in the absence of the laser field. In general, $\chi$ may depend upon the longitudinal coordinate $\eta$, in addition to the transverse coordinates $\rho$ and $\varphi$; here, for simplicity, we assume only a radial dependence. The transverse Laplacian in Eq. (2.1a) accounts for the distortion of the wave-front due to diffraction, the transverse gain variations are described by the function $\chi(\rho)$ and the presence of spherical reflectors is taken into account by the boundary conditions [see Eq. (2.6) below].

The solution of Eqs. (2.1) offers formidable difficulties which we try to remove gradually by recasting the equations in a form that is more amenable to numerical studies and by introducing a number of useful simplifications, chiefly an appropriate generalization of the uniform field limit. Our immediate goal is to derive a set of equations for the field modal amplitudes. For this purpose we consider the expansion

$$F(\rho,\varphi,\eta,\tau) = \sum_{p,m,i} A^{(i)}_{pm}(\rho,\varphi,\eta)\, f^{(i)}_{pm}(\eta,\tau) \qquad (2.4)$$

where the modal functions $A_{pm}^{(i)}$ are given by Eq. (A.23) in Appendix A and obey the orthonormality condition (A.25). A priori, Eq. (2.4) requires consideration of an infinite number of modal amplitudes $f_{pm}^{(i)}$ (p,m = 0,1,2,..; i = 1,2 for m>0) and, in addition, each function $f_{pm}^{(i)}$ depends on $\eta$. However, we anticipate that in the uniform field limit the modal amplitudes become uniform along the longitudinal direction [in a sense that is made precise by Eq. (2.18)] and, moreover, the number of modes that are significantly excited is manageably small.



Upon substituting Eq. (2.4) into (2.1a) and after a few simple steps we arrive at the coupled equations

$$\frac{\partial f^{(i)}_{pm}}{\partial\eta} + \frac{1}{v}\frac{\partial f^{(i)}_{pm}}{\partial\tau} = i\,\frac{\delta\Omega'}{v} f^{(i)}_{pm} - \alpha\Lambda \int_0^{\infty} d\rho\, \rho \int_0^{2\pi} d\varphi\, A^{(i)*}_{pm}(\rho,\varphi,\eta)\, P(\rho,\varphi,\eta,\tau) \qquad (2.5)$$

These are subject to the boundary conditions

$$f^{(i)}_{pm}(-\tfrac{1}{2} f_A,\tau) = R\, e^{-i\delta_{pm}} \exp\left(i\delta\Omega'\gamma_\perp \frac{\Lambda - L_A}{c}\right) f^{(i)}_{pm}\left(\tfrac{1}{2} f_A,\ \tau - \gamma_\perp \frac{\Lambda - L_A}{c}\right) \qquad (2.6)$$

where $f_A \equiv L_A/\Lambda$, and

$$\delta_{pm} = \frac{\omega_{npm} - \omega_{n00}}{c/\Lambda} \qquad (2.7)$$

for any value of the longitudinal mode index n. The cavity eigenfrequencies $\omega_{npm}$ are given by Eq. (A.26) and, by definition, $\delta_{00} = 0$. Our next objective is to recast the boundary conditions (2.6) into a standard periodicity form as a preliminary step to the uniform field limit. As usual,[23] this is accomplished by introducing the new set of independent variables

$$\eta' = \frac{\eta}{f_A} \equiv \frac{z}{L_A} \qquad (2.8a)$$

$$\tau' = \tau + \gamma_\perp \frac{\Lambda - L_A}{c}\left(\frac{\eta}{f_A} + \frac{1}{2}\right) \qquad (2.8b)$$

and the new field amplitudes $\varphi_{pm}^{(i)}$ defined by

$$f^{(i)}_{pm}(\eta',\tau') = \varphi^{(i)}_{pm}(\eta',\tau') \exp\left[-\left(\ln R - i\delta_{pm} + i\delta\Omega'\gamma_\perp \frac{\Lambda - L_A}{c}\right)(\eta' + 1/2)\right] \qquad (2.9)$$

In this way the new field equations take the form

$$\frac{\partial\varphi^{(i)}_{pm}}{\partial\eta'} - \left(\ln R - i\delta_{pm} + i\delta\Omega'\frac{\gamma_\perp\Lambda}{c}\right)\varphi^{(i)}_{pm} + \frac{\gamma_\perp\Lambda}{c}\frac{\partial\varphi^{(i)}_{pm}}{\partial\tau'} = \qquad (2.10)$$

$$-\alpha L_A \exp\left[\left(\ln R - i\delta_{pm} + i\delta\Omega'\gamma_\perp\frac{\Lambda - L_A}{c}\right)(\eta' + 1/2)\right] \int_0^{\infty} d\rho\, \rho \int_0^{2\pi} d\varphi A^{(i)*}_{pm}\, P$$

and the boundary conditions are

$$\varphi^{(i)}_{pm}(-\tfrac{1}{2},\tau') = \varphi^{(i)}_{pm}(\tfrac{1}{2},\tau') \tag{2.11}$$

At this point we assume the uniform field limit

$$\alpha L_A << 1\,, \qquad T \equiv 1 - R << 1 \tag{2.12}$$

where, as usual, the ratio

$$\frac{\alpha L_A}{T} \equiv 2C \tag{2.13}$$

is arbitrary but finite. We also assume that the frequency offset $\delta\Omega'$ is much smaller than the free spectral range, i.e.

$$\delta\Omega' \frac{\gamma_\perp \Lambda}{c} = O(T) \tag{2.14}$$

The main virtue of the uniform field limit is that it sets a strong constraint on the number of modes that can develop an appreciable amplitude, as we now demonstrate with the help of the following argument. We divide the collection of indices (p,m), which label the field modes of interest, into two groups: the first includes the pairs (p,m) for which an integer $M_{pm}$ can be found that satisfies the constraint

$$|\delta_{pm} - 2M_{pm}| = O(T) \tag{2.15}$$

The second group includes all the others for which Eq. (2.15) cannot be satisfied. Note that because $\delta_{00} = 0$, the choice p=m=0 satisfies Eq. (2.15) with $M_{00}$=0 and therefore it belongs to the first group. The physical meaning of this subdivision is that it selects the cavity modes that are nearly degenerate with the reference mode (n=N, p=m=0), or more precisely whose frequency separation from the reference mode is of the order of the cavity linewidth $\kappa = cT/\Lambda$. In fact, as one can verify from Eqs. (A.26) and (2.7), Eq. (2.15) implies that the cavity resonance ($n=N-M_{pm}$,p,m) is nearly degenerate with the reference mode (N,0,0). A graphic representation of this grouping is given in Fig. 2 where we have sketched the position of the first few radial resonances associated with the longitudinal indices N and N-1; in this case the choice (p=3,m=0)



satisfies Eq. (2.15) with $M_{30} = 1$. The significance of this classification becomes especially clear with the help of a result from Ref. 24 concerning the behavior of the steady state solution when the frequency of the laser is close to the reference frequency. In reference 24 we proved that the steady state amplitudes of the non-degenerate modes (i.e. the modes of the second class) are negligible in the uniform field limit, while instead the amplitudes of the modes belonging to the first class have moduli of order unity. Furthermore, if the free spectral range is sufficiently large or, precisely, if

$$\frac{\gamma_\perp \Lambda}{c} \approx T << 1 \tag{2.16}$$

and the ratio

$$\kappa' \equiv \frac{cT}{\Lambda\gamma_\perp} \tag{2.17}$$

is arbitrary, the amplitudes of the second class are negligible also away from the stationary state because the corresponding cavity resonances lie far away from the atomic line. Hence the only modes with any dynamical significance are the quasi-degenerate modes of the first class. In practice, an additional mode selection comes into play in real lasers because transverse modes with larger values of the indices p and m have higher diffraction losses because of the finite size of the mirrors, the limited diameter of the active volume, and the presence of intracavity elements such as pinholes, modulators, etc. As a result, only the lowest order transverse modes are usually involved in the dynamics and therefore we shall limit our considerations to reasonably small upper bounds for the indices p and m.

In Ref. 24 we analyzed the case of radial mode spacing of the order of the free spectral range, assuming that there are no nearly degenerate modes. Under these conditions the laser operates at steady state in a single longitudinal and transverse mode; multimode behavior arises only when the growth of other modes destabilizes the stationary state and produces spontaneous undamped oscillations in the output intensity. If instead the spacing between transverse modes is of the order of the cavity linewidth (i.e. much smaller than the free spectral range) we can anticipate strong mode-mode coupling among the modes of the first class and multimode operation also under steady

state conditions, as a consequence of cooperative frequency locking. The same behavior is expected also when the radial mode spacing is of the order of the free spectral range provided that some of the modes are degenerate or nearly degenerate in the sense of Eq. (2.15), or, more precisely, that the first class includes at least one pair of indices (p,m) different from (0,0). An example is provided by the quasi-confocal resonator where the frequency difference between consecutive transverse resonances is nearly equal to the free spectral range. Also in this case the nearly degenerate modes may lock in frequency and in phase giving rise to multimode stationary configurations. At present, we ignore the issue of diffraction losses which we add phenomenologically at the end of the derivation of the equations of motion.

In summarizing the essence of this discussion, we reiterate that in the uniform field limit (2.12), (2.14) and under the additional assumption (2.16) only quasi-degenerate modes of the first class are dynamically significant; furthermore each set of indices (p.m) in this class is associated with only one value of the longitudinal index, i.e. N-$M_{pm}$. Hence, we conclude that the longitudinal dependence of the modal amplitudes $\varphi_{pm}^{(i)}(\eta',\tau')$ is of the form

$$\varphi_{pm}^{(i)}(\eta',\tau') = \Phi_{pm}^{(i)}(\eta',\tau') \exp\left[-2\pi i M_{pm}(\eta'+1/2)\right] \tag{2.18}$$

where the functions $\Phi_{pm}^{(i)}$ are nearly independent of $\eta'$ in the sense that

$$\frac{\partial \Phi_{pm}^{(i)}}{\partial \eta'} = O(T)$$

and it satisfies the same boundary conditions (2.11) as $\varphi_{pm}^{(i)}$. The new field amplitudes obey the equations of motion

$$\frac{\partial \Phi_{pm}^{(i)}}{\partial \eta'} - \left(\ln R - i\bar{\delta}_{pm} + i\,\delta\Omega'\frac{\gamma_\perp \Lambda}{c}\right)\Phi_{pm}^{(i)} + \frac{\gamma_\perp \Lambda}{c}\frac{\partial \Phi_{pm}^{(i)}}{\partial \tau'} = \tag{2.19}$$

$$= -\alpha L_A \exp\left[\left(\ln R - i\bar{\delta}_{pm} + i\,\delta\Omega'\gamma_\perp \frac{\Lambda - L_A}{c}\right)(\eta'+1/2)\right]\int_0^{\infty} d\rho\,\rho \int_0^{2\pi} d\varphi\, A_{pm}^{(i)*}\, P$$

where



$$\bar{\delta}_{pm} = \delta_{pm} - 2\pi M_{pm} \tag{2.20}$$

Finally we define

$$\psi_{pm}^{(i)}(\tau') = \int_{-1/2}^{+1/2} d\eta'\, \Phi_{pm}^{(i)}(\eta',\tau') \tag{2.21}$$

we integrate the left and right hand sides of Eq. (2.19) with respect to $\eta'$ and carry out the uniform field limit by retaining only the first order terms in T and $\alpha L_A$. The result is

$$\frac{\partial \psi_{pm}^{(i)}}{\partial \tau'} = -\kappa'(1 + i a_{pm} - i\,\delta\Omega'/\kappa')\,\psi_{pm}^{(i)} - 2C\kappa' \int_{-1/2}^{+1/2} d\eta' \int_0^{\infty} d\rho\,\rho \int_0^{2\pi} d\varphi\, A_{pm}^{(i)*}(\rho,\varphi,\eta')\, P \tag{2.22}$$

where we have defined

$$a_{pm} = \frac{\bar{\delta}_{pm}}{T} \tag{2.23}$$

and $\kappa'$ is the cavity linewidth in units of $\gamma_\perp$ (see Eq. (2.17). Also, for definiteness, we select $\delta\Omega'$ as the value given by the standard mode-pulling formula, so that [see for example Ref. 23]

$$\frac{\delta\Omega'}{\kappa'} = \frac{\delta'_{AC}}{1+\kappa'} = \Delta' \tag{2.24}$$

A further convenient simplification arises if we can assume that

$$L_A << \Lambda\eta_1 \tag{2.25}$$

where $\Lambda\eta_1$ is the Raileigh length of the cavity field in the region occupied by the active medium. In this case, for $-1/2 \le \eta' \le 1/2$ we have

$$A_{pm}^{(i)}(\rho,\varphi,\eta') = A_{pm}^{(i)}(\rho,\varphi,0) \equiv A_{pm}^{(i)}(\rho,\varphi) \tag{2.26}$$

and the required equations of motion take the form

$$\frac{\partial \psi_{pm}^{(i)}}{\partial \tau'} = -\kappa'(1 + i a_{pm} - \Delta')\,\psi_{pm}^{(i)} - 2C\kappa' \int_0^{\infty} d\rho\,\rho \int_0^{2\pi} d\varphi\, A_{pm}^{(i)}(\rho,\varphi)\, P(\rho,\varphi,\tau') \tag{2.27a}$$

$$\frac{\partial P}{\partial \tau'} = - \left[ FD + (1+i\Delta')P \right] \tag{2.27b}$$

$$\frac{\partial D}{\partial \tau'} = - \gamma \left[ - \tfrac{1}{2} (F^* P + F P^*) + D - \chi(\rho) \right] \tag{2.27c}$$

with

$$F(\rho,\varphi,\tau') = \sum_{pmi} A^{(i)}_{pm}(\rho,\varphi)\, \psi^{(i)}_{pm}(\tau') \tag{2.28}$$

We note that in terms of a new radial variable ρ',defined by

$$\rho' = \frac{\rho}{\sqrt{\eta_1}} \tag{2.29}$$

and after introducing the scaled functions

$$\bar{\psi}^{(i)}_{pm} = \frac{\psi^{(i)}_{pm}}{\sqrt{\eta_1}} \tag{2.30}$$

and

$$\bar{A}^{(i)}_{pm}(\rho',\varphi) = 2(2\rho'^2)^{m/2} \sqrt{\frac{p!}{(p+m)!}}\, L^m_p(2\rho'^2) \exp(-\rho'^2)\, B_m(\varphi) =$$

$$= \sqrt{\eta_1}\; A^{(i)}_{pm}(\rho',\varphi) \tag{2.31}$$

Eqs. (2.27) retain exactly the same form in terms of the new variables; this is also true for the orthogonality relation (A.25). In this way the parameter $\eta_1$ is no longer explicitly in evidence in the working equations. Thus, in summary, the basic equations of the model are

$$\frac{\partial \bar{\psi}^{(i)}_{pm}}{\partial \tau'} = - \kappa' (1 + i a_{pm} - i\Delta')\, \bar{\psi}^{(i)}_{pm} - 2C\kappa' \int_0^{\infty} d\rho'\, \rho' \int_0^{2\pi} d\varphi\, \bar{A}^{(i)}_{pm}\, P \tag{2.32a}$$

$$\frac{\partial P}{\partial \tau'} = - \left[ FD + (1+i\Delta')\, P \right] \tag{2.32b}$$

$$\frac{\partial D}{\partial \tau'} = - \gamma \left[ - \tfrac{1}{2} (F^* P + F P^*) + D - \chi(\rho') \right] \tag{2.32c}$$



where

$$F(\rho',\varphi,\tau') = \sum_{pmi} \bar{A}^{(i)}_{pm}(\rho',\varphi)\, \bar{\psi}^{(i)}_{pm}(\tau') \tag{2.33}$$

and

$$\int_0^{\infty} d\rho'\, \rho' \int_0^{2\pi} d\varphi\, \bar{A}^{(i)\,*}_{pm}(\rho',\varphi)\, \bar{A}^{(i')}_{p'm'}(\rho',\varphi) = \delta_{pp'}\delta_{mm'}\delta_{ii'} \tag{2.34}$$

Two interesting remarks are appropriate when the frequency spacing between transverse modes with the same value of the longitudinal index is of the order of the cavity linewidth (this implies that $M_{pm}$ is equal to zero for all values of p and m under consideration). First, the assumption (2.25) becomes a consequence of (2.15) because the latter condition together with Eqs. (2.7) and (A.26) implies that $\eta_1 = O(1/T) >> 1$ and therefore $L_A << \Lambda\eta_1$. Second, one can reformulate Eq. (2.32a) as an equation for the entire field amplitude F [Eq. (2.28)]. In fact, consider the identity

$$\left( \frac{i}{4} \nabla'^2_{\perp} - \rho'^2 \right) \bar{A}^{(i)}_{pm} = - (2p+m+1)\, \bar{A}^{(i)}_{pm} \tag{2.35}$$

where

$$\nabla'^2_{\perp} = \frac{\partial^2}{\partial \rho'^2} + \frac{1}{\rho'} \frac{\partial}{\partial \rho'} + \frac{1}{\rho'^2} \frac{\partial^2}{\partial \varphi^2} \tag{2.36}$$

With the help of Eqs. (2.23), (2.7) and (A.26) and by exploiting the completeness of the set of functions $\bar{A}_{pm}(i)$, one obtains from Eqs. (2.32), (2.28), (2.30) and (2.31)

$$\frac{\partial F}{\partial \tau'} = - \kappa' \left[ 1 - i\Delta' - i \frac{a}{2} \left( \frac{i}{4} \nabla'^2_{\perp} - \rho'^2 + 1 \right) \right] F - 2C\kappa' P(\rho',\varphi,\tau') \tag{2.37}$$

where

$$a = \frac{4}{T} \left[ \tan^{-1} \frac{1-f}{2\eta_2} + \tan^{-1} \frac{f}{2\eta_1} \right] \tag{2.38}$$

## 3. Numerical study of the equations of motion

For the purpose of numerical work it is convenient to expand the atomic variables P and D that appear in Eqs. (2.32) in terms of the complete set of modal functions $\bar{A}_{pm}^{(i)}(\rho',\varphi)$ defined in Eq. (2.31). Thus we let

$$P(\rho',\varphi,\tau') = \sum_{pmi} \bar{A}_{pm}^{(i)}(\rho',\varphi)\, p_{pm}^{(i)}(\tau') \tag{3.1a}$$

$$D(\rho',\varphi,\tau') = \sum_{pmi} \bar{A}_{pm}^{(i)}(\rho',\varphi)\, d_{pm}^{(i)}(\tau') \tag{3.1b}$$

and with the help of the orthogonality relations (2.34) we obtain

$$\frac{\partial \bar{\psi}_{pm}^{(i)}}{\partial \tau'} = -\kappa'(1 + ia_{pm} - i\Delta')\,\bar{\psi}_{pm}^{(i)} - 2C\kappa' p_{pm}^{(i)} \tag{3.2a}$$

$$\frac{\partial p_{pm}^{(i)}}{\partial \tau'} = -\Big\{\sum_{p'm'i'}\sum_{p''m''i''} \Gamma(\sigma,\sigma',\sigma'')\,\bar{\psi}_{p'm'}^{(i')}\, d_{p''m''}^{(i'')} + (1+i\Delta')\, p_{pm}^{(i)}\Big\} \tag{3.2b}$$

$$\frac{\partial d_{pm}^{(i)}}{\partial \tau'} = -\gamma\Big\{-\tfrac{1}{2}\Big(\sum_{p'm'i'}\sum_{p''m''i''} \Gamma(\sigma,\sigma',\sigma'')\,\bar{\psi}_{p'm'}^{(i')\,*}\, p_{p''m''}^{(i'')} + \text{c.c.}\Big) + d_{pm}^{(i)} - \chi_{pm}^{(i)}\Big\} \tag{3.2c}$$

where $\sigma$ is a short-hand notation for (p,m,i) and

$$\Gamma(\sigma,\sigma',\sigma'') = \int_0^\infty d\rho'\,\rho' \int_0^{2\pi} d\varphi\, \bar{A}_{pm}^{(i)}\, \bar{A}_{p'm'}^{(i')}\, \bar{A}_{p''m''}^{(i'')} \tag{3.3a}$$

$$\chi_{pm}^{(i)} = \int_0^\infty d\rho'\,\rho' \int_0^{2\pi} d\varphi\, \bar{A}_{pm}^{(i)}\, \chi(\rho') \tag{3.3b}$$

The field damping term $-\kappa'\bar{\psi}_{pm}^{(i)}$ that appears on the right hand side of Eq. (3.2a) is a consequence of the partial reflectivity of the cavity output couplers; in this form, Eq.(3.2a) assigns the same loss rate to every field modal amplitude. In practice, however, higher order transverse modes are more heavily damped than their lower order counterparts because of the limited transverse dimensions of



the resonator and the possible presence of intracavity elements such as pinholes, modulators, etc. The simplest way to account for this additional loss mechanisms is to replace the damping term $-\kappa'\bar{\psi}_{pm}^{(i)}$ with $-\kappa_{pm}'\bar{\psi}_{pm}^{(i)}$ and to select $\kappa_{pm}'$ as an appropriate monotonically growing function of the indices (p,m). This artifice has the advantage of further reducing the number of dynamically relevant modal amplitudes and to bring the model more in line with realistic laser systems.

We begin our survey of the numerical solutions of Eq. (3.2) by focusing first on the behavior of the model under the assumption that cylindrical symmetry prevails during the laser action. This regime can be enforced rather easily in typical experimental situations.[21] Under conditions of cylindrical symmetry, the modal index m is equal to zero and the index (i) must be dropped from all the modal amplitudes in Eqs. (3.2) which now take the form

$$\frac{\partial \bar{\psi}_p}{\partial \tau'} = -\kappa_p'\bar{\psi}_p - i\kappa'(a_p - \Delta')\,\bar{\psi}_p - 2C\kappa' p_p \tag{3.4a}$$

$$\frac{\partial p_p}{\partial \tau'} = -\Big\{\sum_{p'p''} \Gamma_{pp'p''}\,\bar{\psi}_{p'}\, d_{p''} - (1+i\Delta')\, p_p\Big\} \tag{3.4b}$$

$$\frac{\partial d_p}{\partial \tau'} = -\gamma\Big\{-\tfrac{1}{2}\Big(\sum_{p'p''} \Gamma_{pp'p''}\,\bar{\psi}_{p'}^{*}\, p_{p''} + \text{c.c.}\Big) + d_p - \chi_p\Big\} \tag{3.4c}$$

The modal functions of the resonator are

$$\bar{A}_p(\rho') = 2L_p(2\rho'^2)\exp(-\rho'^2) \tag{3.5}$$

where for simplicity we have dropped the factor $B_0 = (2\pi)^{-1/2}$ so that the orthonormality relation takes the form

$$\int_0^\infty d\rho'\,\rho'\,\bar{A}_p(\rho')\,\bar{A}_q(\rho') = \delta_{pq}$$

The mode-mode coupling coefficients $\Gamma_{pp'p''}$, given by Eq. (B.1) can be calculated with the help of a simple recursion relation developed in Appendix B. For definiteness, and somewhat arbitrarily, we have chosen

$$\kappa_p' = \kappa' g_p, \qquad g_p = 1 + \beta p^4, \qquad (p = 0, 1, 2,..) \tag{3.6}$$

where $\beta$ is a constant and, in addition, we have assumed a uniform pump profile for the active medium; with this selection, the equilibrium modal populations are given by the simple formula

$$\chi_p = (-1)^p \tag{3.7}$$

We note that, in the case of a cavity with quasi-planar mirrors in which the frequency spacing between transverse modes with the same value of the longitudinal index n is of the order of the cavity linewidth, one has the simple relation

$$a_p = a_1 p \tag{3.8}$$

where $a_1 = a$ is given by Eq. (2.38). This is easily seen if we consider that in this case $M_p$ in Eq. (2.15) vanishes, and if we use Eq. (2.23) with $\bar{\delta}_p = \delta_p$ [see Eq. (2.20)], Eq. (2.7), and Eq. (A.21). In the case of a quasi-confocal cavity, instead, the quasi-degenerate modes have different values of the longitudinal index n, and $M_p = p$. Again Eq. (3.8) holds true, provided we define the parameter $a_1$ as

$$a_1 = \delta_1 - 2\pi \tag{3.9}$$

Hence the two cases of a quasi-planar and quasi-confocal cavity can be treated simultaneously with the same set of Eqs. (3.4), keeping Eq. (3.8) into account; the quasi-planar (confocal) configuration corresponds to values $a_1 \geq 0$ ($a_1 \leq 0$). In our calculations we will consider only the quasi-planar case in which the dynamics is governed by the single value n = N of the longitudinal index and where $a_1$ denotes the frequency spacing between adjacent transverse modes, measured in units of the cavity linewidth $\kappa$. In the following, for simplicity, we will refer to the parameter $a_1$ as the frequency spacing.

The other parameters of the model (3.4) and their values selected for the simulations are:

- the ratio $\kappa'$ of the cavity linewidth $\kappa$ to the atomic linewidth $\gamma_\perp$ [set equal to 1.0 (case a) or equal to 0.3 (case b)];
- the ratio $\gamma$ of the relaxation rate $\gamma_\parallel$ of the population inversion to the atomic linewidth $\gamma_\perp$ (set equal to 0.05);
- the parameter $\beta$ which governs the effective losses of the transverse modes [Eq. (3.6)] (set equal to 0.005);
- the pump parameter C (set equal to 1.2);
- the atomic detuning parameter $\Delta'$ which is defined by Eq. (2.24), where $\delta_{AC}$ is the difference between the atomic transition frequency $\omega_A$ and the frequency $\omega_0$ of the fundamental mode, measured in units of $\gamma_\perp$ (set equal to 0.18).



Before entering the details of the numerical simulations, we consider the steady state solutions. In the case in which only one mode dominates over the others, the stationary solution can be shown analytically to be given by [20]

$$\mathrm{Re}(\bar{\psi}_p^{st}) = \left\{ \frac{1}{\Gamma_p g_p} \left[ 2C - g_p \{ 1 + (\Delta' - \varepsilon)^2 \} \right] \right\} \tag{3.10a}$$

$$\mathrm{Im}(\bar{\psi}_p^{st}) = 0 \tag{3.10b}$$

$$\varepsilon = \frac{\kappa' a_p}{1 + \kappa'} \tag{3.10c}$$

$$\Gamma_p = \sum_q \Gamma_{ppq} \Gamma_{qpp} = 4 \int_0^\infty dx\, e^{-2x} \left( L_p(x) \right)^4 \tag{3.10d}$$

where $\varepsilon$ is the shift in units of $\gamma_\perp$ between the operating laser carrier and the reference frequency and the arbitrary phase of the electric field has been set equal to zero. These solutions are stable only if the spacing between transverse modes is sufficiently large as compared to $\kappa$, the p-mode resonance is the closest to the atomic frequency and the atomic linewidth $\gamma_\perp$ is of the same order as $\kappa$. A first step in understanding multimode operation is to consider a situation where only two modal amplitudes are different from zero. By reducing the frequency spacing, modes with higher modal index increase their gain and, since they make better use of the available population inversion, they induce a process of competition with other transverse modes. The outcome of this competition cannot be known a priori as the modes with higher modal index also experience higher diffraction losses. We consider, for example, the competition between the modes p=0 and p=1,

even if the following calculations can be extended to any pair of successive tranverse modes. The cumbersome algebraic expression of the steady state solution close to the lasing threshold is reported in the Appendix C. For large values of $a_1$ a single Gaussian solution (p=0) is stable and the laser carrier is tuned to the reference frequency. By taking advantage of the fact that the laser is close to threshold, we perform a perturbative expansion of Eqs. (C.2-5) and obtain an analytical expression for the shift of the laser frequency

$$\varepsilon = \frac{\kappa'(2C - 1 - \Delta'^2)(a_1 + \Delta'\beta)}{4(1 + \kappa')(1 + \Delta'^2)(a_1^2 + \beta^2)} \qquad (3.11)$$

A comparison between Eq. (3.11) and the corresponding value calculated by direct integration of Eqs. (3.4) is shown in Fig. 3. The slight mismatch between the two curves is due to the selected value of the gain which does not quite fulfill the perturbative condition. The growing p=1 mode pulls the laser frequency toward its characteristic resonance without, however, generating a beat note over a large range of values of $a_1$. The departure of the curve (b) in Fig. 3 from the behavior described by Eq. (3.11) (curve (a)) is the signature of the onset of oscillations which characterize the dynamics for sufficiently smaller values of the control parameter $a_1$.

We have carried out our numerical simulations by fixing the parameter $\beta$ to 0.005 which selects p=3 as the largest significant modal index for the chosen gain. However, in order to insure a satisfactory convergence of the integration process, we have included all modes up to p=7 for field and polarization and up to p=10 for the population inversion. We have also controlled a posteriori that the amplitude of the mode p=7 had remained at least three orders of magnitude smaller than that of the mode p=3.

A physical quantity that characterizes the global dynamical behavior of the laser is the total flux

$$\Phi(t) = 2\pi \int_0^\infty d\rho\, \rho\, |E(\rho,t)|^2 = 2\pi \sum_p |\bar{\psi}_p(t)|^2 \qquad (3.12)$$

whose evolution for decreasing values of $a_1$ is shown in Fig. 4 for both cases of $\kappa'=1.0$ (curve a)



and $\kappa'=0.3$ (curve b). We observe two major regions of instability alternating with time-independent regimes of cooperative frequency locking.[19,20] In the latter state, the modes select a common frequency of operation which generally lies close to the characteristic resonance of the largest mode. In this way we can identify the first region of instability as a competition for the same population inversion, between the p=0 and the growing p=1 mode. Once the p=1 mode dominates over the others, a new cooperative frequency locked state is reached and the laser frequency is sligtly detuned from the p=1 resonance. A mechanism similar to the pulling described by Eq. (3.11), rules the onset of the second instability region when the p=2 mode grows above a particular threshold. This picture of alternating locking and unlocking regions is shown in better evidence in Fig. 5 where the amplitudes of the p=0,1,2 modes are reported for the two cases a) and b) of Fig. 4.

The detailed nature of the oscillations in the second region of instability depends on the losses of the laser. For larger values of the ratio $\kappa'=\kappa/\gamma_\perp$ we have observed more complicate oscillatory behaviors such as quasiperiodic and chaotic motions. These complicated oscillations disappear if we lower the losses of the cavity, a feature which is in line with the experimental results reported in Ref. 21 with a $CO_2$ laser. Transverse sections of the beam profile are shown in Fig. 6 for the $\kappa'=1.0$ in the periodic, quasiperiodic and chaotic states. Quasiperiodic and dynamically locked states are to be expected because of the simultaneous frequency pulling induced by each one of the three active modes. However the new and more interesting behavior is the gradual increase of complexity in the spatio-temporal solutions when we decrease the control parameter $a_1$. In order to characterize the complexity of these solutions we have calculated the intensity correlation function

$$C_{max}(0,\rho) = \mathrm{Max}(\forall\delta\tau)\, \frac{\langle I(0,\tau)\, I(\rho,\tau+\delta\tau)\rangle - \langle I(0,\tau)\rangle\langle I(\rho,\tau)\rangle}{\sigma(0)\,\sigma(\rho)} \qquad (3.13)$$

where $I(\rho)$ is the field intensity at distance $\rho$ from the center of the beam, $\sigma(\rho)$ is the standard deviation of $I(\rho)$ and the brackets indicate a time average. Among the relevant properties of this correlation function, we mention that $C_{max}(0,\rho)$

(i) is properly normalized over the interval (0,1),

(ii) is equal to unity for signals calculated at different radial locations which are merely dephased in time relative to one another, and

(iii) is equal to unity for oscillating signals that are produced by beat notes.

Figure 7 shows $C_{max}(0,\rho)$ for the three spatio-temporal solutions of Fig. 6. The progressive decrease of the spatial correlation is in agreement with the increased complexity of the patterns. Work is presently in progress to connect this phenomenon with the presence of singularities of the solutions and the possible appearance of defects.[36]

## 4. A discussion of cooperative frequency locking

We have introduced the descriptor "cooperative frequency locking" to denote a regime of operation in which two or more modes oscillate in synchronism with fixed relative phases and generate a time-independent output intensity. Because our analysis of this phenomenon is based on the concept of empty cavity modes, one might raise the objection that a more accurate approach ought to involve basis functions that can account for the presence of the nonlinear active medium. In answer to this objection, we stress that the empty cavity modes provide an asymptotically exact representation of the laser field in the limit in which $\alpha L_A << 1$, the limit of interest to this paper. Nevertheless, there still remain some subtle problems which require a more careful discussion.

When dealing, for example, with a linear chain of harmonic oscillators we can describe their motion either in terms of their individual coordinates and momenta or by the normal mode variables which are dynamically decoupled from each another and correspond to well defined renormalized or dressed frequencies. A state of the system in which one normal mode is excited can be thought of as a multimode configuration in terms of the original variables, or as a single-mode configuration in terms of dressed states of the interacting system. In the same way one may suggest that the cooperative frequency locked states are just dressed normal modes of the laser, an interpretation that greatly reduces the significance of this phenomenon. The main goal of this section is to suggest that this interpretation is not appropriate for the nonlinear system of interest to this work.



In our investigations of cooperative frequency locking we have focused on two distinct types of optical resonators: Cartesian cavities with lateral mirrors, as in Ref. 19, and more conventional resonators with spherical output couplers, as in this work. In the former case, where the empty cavity modes are labelled by the index n=0,1,2,..., we can recognize two different groups of stationary solutions. The solutions of the first group, which include also the homogeneous stationary state, are numbered by an index k=0,1,2... and can be recognized by the fact that the only modes with appreciable amplitude are the modes n=k, the third, sixth, etc. harmonics [i.e., for each solution the nonzero modal components correspond to the indices n=(2s+1)k, with s=0,1,2,...]. It follows that the solution labelled k=0 has only the mode n=0 excited, while for k≠0 the mode n=0 is altogether absent. The solutions of the second group, instead, are such that the mode n=0 coexists with a number of other modes with n≠0.

With this in mind, it is reasonable to consider the solutions of the first group as some kind of dressed normal modes of the nonlinear system because of the admixture of the fundamental component n=k and its harmonics caused by the nonlinear interaction (we might mention however that the dressing effects is rather small because the amplitude of the n=k mode is much larger than those of its harmonics). The solutions of the second group represent something altogether different from a simple dressing effect. The cooperative frequency locking is associated precisely with solutions of the latter type where no single mode has a dominant character.

For the case of resonators with spherical mirrors each mode is coupled to all the others by the nonlinear interaction; the problem is much more complicated and, apparently, does not allow a simple classification of the stationary solutions. Yet, even in this case, we can still advance a simple physical interpretation of the numerical results in terms of empty cavity modes. We have seen instances in which the system approaches a steady state and one of the modes dominates over the others. These situations can be interpreted as single-mode behaviors, or as a kind of injection locking induced by the dominant modal component.

We have also seen several cases where the presence of several modes with comparable amplitudes creates a greater level of competition. Sometimes, under these conditions, the output

intensity acquires an oscillatory behavior which is easily traced to the interference among the competing modes from the fact that the oscillation frequency is equal to the mode-pulled intermode spacing. When the number of dominant modes is larger than two, a periodic output implies that the modes are able to maintain the mode-locked arrangement, which is typical of homogeneously broadened systems. Symmetry breaking can also occur due to the nonlinear coupling and when this happens the output intensity oscillations acquires a quasi periodic or chaotic character.

There are also parameter values where several modes with comparable amplitudes switch from a competitive to a cooperative behavior and produce phase and frequency locked configurations in which the output intensity becomes stationary just as in the case of single-mode operation. An essential requirement for the appearance of this phenomenon is that the relevant empty cavity modes be quasi-degenerate or, better, that their frequency spacing be of the order of the cavity linewidth. This is what we call cooperative frequency locking. From this perspective we believe that this phenomenon has a highly nontrivial origin and cannot be easily interpreted as the consequence of a simple dressing operation induced by the nonlinear interaction.

## 5. Conclusion

The main objective of this paper was to derive a set of equations for the description of laser dynamics in the presence of transverse effects, and to present the most interesting predictions of this model. The inclusion of transverse degrees of freedom in the traditional Maxwell-Bloch formulation is responsible for a much greater level of complexity than one finds in the plane-wave counterpart models. Hence, our aim was to identify a sufficiently realistic set of conditions that would allow us to focus on the essential features of the transverse dynamics without requiring, at the same time, extensive numerical computations. A suitable extension of the plane-wave uniform field limit to the case in which transverse effects become important turns out to be a very satisfactory solution for this problem. In fact, under the assumptions of this model, the cavity modes fall naturally into two classes: one contains those few modes whose amplitudes grow to appreciable values, the other includes the modes whose excitation remains negligible for all times.



The uniform field limit allows a natural selection of the relevant modal equations which are now few enough in number that one can entertain small-scale numerical simulations for their solution. This selection process is sharpened, in addition, by the existence of diffraction losses in the resonator which grow with the transverse indices of the cavity modes. Finally, in this limit the essential part of the modal amplitudes of the field are almost uniform longitudinally so that their evolution is governed by an ordinary set of time-dependent differential equations.

In this study we have assumed that the set of modes that can develop an appreciable amplitude include the mode (N,0,0). Of course this is not always the case, and one can easily generalize this treatment to the situation where the mode (N,P,M) develops an appreciable amplitude and derive a set of time evolution equations for the amplitudes of the mode (N,P,M) and of those that are nearly degenerate with it. In this case it is best to select the frequency of the (N,P,M) mode as the reference frequency.

The solutions presented in this work show the existence of stationary and time-dependent regimes: the most interesting stationary states correspond to mixtures of cavity modes whose frequencies, in the absence of an active medium, differ from each other. These modes attain a steady state oscillation without beat phenomena through a process called cooperative frequency locking, in which the individual amplitudes develop a synchronous behavior and produce a total field characterized by a single carrier frequency which is common to all. The time dependent configurations exhibit the expected variety of behaviors with periodic, quasi-periodic or even chaotic oscillations. This is expected because the strong interaction among transverse modes develops henever their natural frequencies are in close proximity of one another.

We have analyzed the spatial behavior of the intensity patterns at the output of the laser under time dependent conditions and attempted to characterize the various levels of spatial complexity. This is a problem that has received somewhat limited attention thus far and which deserves to be investigated at much greater depth. One of the open issues, and arguably the most obvious, is suggested at once by the very existence of numerous diagnostic tools for the analysis of temporal complexity: how can one develop, in a parallel way, suitable indices for the characterization of

spatial complexity? Here we have tried to answer this question in a preliminary way by introducing an appropriate spatial correlation function for the output intensity. A seemingly curious feature of this function is that its modulus, for each pair of radial positions, acquires its largest value for a non-zero time delay. This suggests the existence of correlated wave-like phenomena that propagate across the transverse profile of the beam at a finite speed. With the chosen definition, our correlation function consistently decays from unity when the output intensity patterns become more complex.

There are additional ramifications to be studied such as the possible connection of these features with the notion of defects. These issues, however, are still too preliminary to be discussed at this point.



## Appendix A - The modal structure of the ring resonator

A schematic representation of the typical unidirectional ring resonator of interest to this work is shown in Fig. 8. The length of the cavity is $\Lambda$ and the two spherical mirrors have the same radii of curvature $R_0$ and power reflectivity R. Their separation is denoted by L. In order to keep our calculations as simple as possible, we consider first the case in which the cavity field has cylindrical symmetry,[37] i.e. it depends only on the radial coordinate r, the longitudinal coordinate z and the time. In this case the field obeys the wave equation

$$\nabla^2 E(r,z,t) - \frac{1}{c^2}\frac{\partial^2}{\partial t^2} E(r,z,t) = 0 \qquad (A.1)$$

where

$$\nabla^2 \equiv \frac{\partial^2}{\partial r^2} + \frac{1}{r}\frac{\partial}{\partial r} + \frac{\partial^2}{\partial z^2} \qquad (A.2)$$

and r is the radial coordinate along a direction transverse to the longitudinal axis of the resonator. In the paraxial approximation we seek elementary solutions of the form

$$E(r,z,t) = A(r,z)\exp[i(kz - \omega t)] \qquad (A.3)$$

where A(r,z), a slowly varying function of z, is a solution of the equation

$$\left(\frac{\partial^2}{\partial r^2} + \frac{1}{r}\frac{\partial}{\partial r}\right)A(r,z) + 2ik\frac{\partial}{\partial z}A(r,z) = 0 \qquad (A.4)$$

and $k = \omega/c$. In terms of the scaled coordinates

$$\eta = \frac{z}{\Lambda}, \qquad \rho = \sqrt{\frac{\pi}{\Lambda\lambda}}\, r \qquad (A.5)$$

we have

$$\frac{\partial A}{\partial \eta} = \frac{i}{4}\left(\frac{\partial^2}{\partial \rho^2} + \frac{1}{\rho}\frac{\partial}{\partial \rho}\right)A \qquad (A.6)$$

We divide the ring resonator in successive longitudinal segments bounded by pairs of curved mirrors. In the example of Fig. 8 there are two such segments, labelled 1 and 2 in the figure (if the plane mirror were replaced by a curved reflector, the cavity would have to be divided into three

parts). The solution of Eq. (A.6) over the range $-L/(2\Lambda) \le \eta \le L/(2\Lambda)$ is given by

$$A^{(1)}(\rho,\eta) = \frac{2}{v(\eta)} L_p\left(\frac{2\rho^2}{v^2(\eta)}\right) \exp\left(-\frac{\rho^2}{v^2(\eta)} + i\frac{\rho^2}{u(\eta)}\right) \exp\left(-i(2p+1)\tan^{-1}\eta/\eta_1\right) \qquad (A.7)$$

where $L_p$ ($p = 0,1,2...$) is the Laguerre polynomial of order p and the indicated argument,

$$v(\eta) = \sqrt{\eta_1}\ \left[1 + (\eta/\eta_1)^2\right]^{1/2} \qquad (A.8a)$$

represents the beam waist at the position $\eta$, and

$$u(\eta) = \frac{1}{\eta}(\eta_1^2 + \eta^2) \qquad (A.8b)$$

measures the scaled radius of curvature of the wavefront. The parameter $\eta_1$ is arbitrary at this point and must be specified with the help of the cavity boundary conditions; in the chosen system of units $\eta_1$ plays the role of the Rayleigh length of the beam (i.e. the distance between the two transverse planes where the beam waist is larger than the minimum size by a factor $\sqrt{2}$), while

$$\sqrt{\eta_1} = v(0) \qquad (A.8c)$$

is the minimum waist size.

The solution of Eq. (A.6) for any other segment of the resonator has the same formal structure as Eq. (A.7) except for the value of the minimum waist, which is usually different in every segment, and for an extra phase factor which is needed to join the solutions smoothly with one another. Thus in region 2 we have

$$A^{(2)}(\rho,\eta) = \frac{2}{\alpha(\eta)} L_p\left(\frac{2\rho^2}{\alpha^2(\eta)}\right) \exp\left(-\frac{\rho^2}{\alpha^2(\eta)} + i\frac{\rho^2}{\beta(\eta)}\right) x$$

$$\exp\left[-i\,(2p+1)\tan^{-1}\frac{\eta - 1/2}{\eta_2}\right] \exp(i\varphi) \qquad (A.9)$$

where

$$\alpha(\eta) = \eta_2\left[1 + \left(\frac{\eta - 1/2}{\eta_2}\right)^2\right]^{1/2} \qquad (A.10a)$$



$$\beta(\eta) = \frac{1}{\eta - 1/2}\left[(\eta - 1/2)^2 + \eta_2^2\right] \qquad (A.10b)$$

and $\varphi$ is a phase factor that must be adjusted to fit the boundary conditions. The shift of the longitudinal coordinate that appears in Eqs. (A.10) is made in conformity with the chosen origin of the $\eta$ axis.

These Gauss-Laguerre solutions, as they are called, are characterized by the beam parameter $q(\eta)$ defined by

$$\frac{1}{q(\eta)} = \frac{1}{u(\eta)} + i\frac{1}{v^2(\eta)} \qquad (A.11)$$

This complex quantity satisfies elementary mapping rules under translation and reflection from a spherical mirror.[38] If $q_1$ is any beam parameter, the translated and reflected values are given, respectively, by

i) $$q_2 = q_1 + d \qquad (A.12a)$$

and

ii) $$q_2 = \frac{q_1}{-\frac{2}{\rho_0} q_1 + 1} \qquad (A.12b)$$

where d is an arbitrary length (in units of $\Lambda$) and $\rho_0 = R_0/\Lambda$ is the scaled radius of curvature of the mirrors. With the help of these rules we can follow the variations of the Gauss-Laguerre beam at every point along the resonator.

In order to complete the solution of our problem we must calculate the parameters $\eta_1$ and $\eta_2$ and the phase factor $\varphi$ in terms of the cavity geometry, and derive an expression for the empty cavity eigenfrequencies. The calculation of $\eta_1$ proceeds as follows: let $q(\eta=0)$ denote the beam parameter at $\eta=0$; we propagate this value and reflect it as many times as needed until we complete a full loop. At the end, we require that the final beam parameter $q(\eta=1)$ coincide with $q(\eta=0)$. We let

$$f = \frac{L}{\Lambda}$$

and we have

$$q(\eta=0) = -iv^2(0) = -i\eta_1 \tag{A.13a}$$

$$q(\eta = \tfrac{1}{2} f - \varepsilon) = q(\eta = 0) + \tfrac{1}{2} f \tag{A.13b}$$

$$q(\eta = \tfrac{1}{2} f + \varepsilon) = \frac{q(\eta = \frac{1}{2} f - \varepsilon)}{-\frac{2}{\rho_0} q(\eta = \frac{1}{2} f - \varepsilon) + 1} \tag{A.13c}$$

etc..

$$q(\eta = 1) = q(\eta = 1 - \tfrac{1}{2} f + \varepsilon) + \tfrac{1}{2} f \equiv q(\eta = 0) \tag{A.13d}$$

where $-\varepsilon$ and $+\varepsilon$ indicate positions just before and after reflection by the spherical mirrors.

The solution of this simple set of equations is

$$\eta_1 = \frac{1}{2} \sqrt{\frac{(\rho_0 - f)(\rho_0 + f^2 - f)}{\rho_0 + f - 1}} \tag{A.14}$$

subject to the constraint $\rho_0 + f - 1 > 0$. In a similar way we can propagate the initial beam parameter (which is now known) up to point $\eta = 1/2$ of Fig. 8 and arrive at

$$\eta_2 = \frac{1}{\rho_0^2 \eta_1} \left\{ \eta_1^2 (1 - f - \rho_0)^2 + \tfrac{1}{4} (\rho_0 + f^2 - f)^2 \right\} \tag{A.15}$$

Now we must impose the boundary conditions at each curved mirror (reflections at plane surfaces are assumed to leave the beam invariant). In the paraxial approximation the reflection at a spherical mirror is approximately equivalent to a multiplication by the phase factor

$$\Re = \exp(-i \frac{2\rho^2}{\rho_0}) \tag{A.16}$$

Thus we impose that

$$\Re\, E^{(1)}(\eta = \tfrac{1}{2} f - \varepsilon, \rho, t) = E^{(2)}(\eta = \tfrac{1}{2} f + \varepsilon, \rho, t) \tag{A.17}$$

We observe that



$$v^2(\eta = \tfrac{1}{2} f - \varepsilon) = u^2(\eta = \tfrac{1}{2} f + \varepsilon) \tag{A.18a}$$

$$-\frac{2}{\rho_0} + \frac{1}{u(\eta = \frac{1}{2} f - \varepsilon)} = \frac{1}{\beta(\eta = \frac{1}{2} f + \varepsilon)} \tag{A.18b}$$

With the help of these relations and of Eqs. (A.3), (A.7) and (A.16) it is easy to verify that the first boundary condition (A.17) is satisfied if

$$\varphi = -(2p+1) \left[ \tan^{-1} \frac{f}{2\eta_1} + \tan^{-1} \frac{1 - f}{2\eta_2} \right] \tag{A.19}$$

Now we impose the boundary condition at the second curved mirror, i.e.

$$\Re\, E^{(2)}(\eta = 1 - \tfrac{1}{2} f - \varepsilon, \rho, t) = E^{(1)}(\eta = -\tfrac{1}{2} f + \varepsilon, \rho, t) \tag{A.20}$$

and arrive at the required result

$$\omega_{n,p} = \frac{2\pi c}{\Lambda} n + \frac{2c}{\Lambda} (2p+1) \left[ \tan^{-1} \frac{1 - f}{2\eta_2} + \tan^{-1} \frac{f}{2\eta_1} \right] \tag{A.21}$$

$n,p = 0, 1, 2, \ldots$

The inclusion of the angular dependence requires only a few modifications. The transverse Laplacian is now given by

$$\nabla_\perp^2 = \frac{\partial^2}{\partial \rho^2} + \frac{1}{\rho} \frac{\partial}{\partial \rho} + \frac{1}{\rho^2} \frac{\partial^2}{\partial \varphi^2} \tag{A.22}$$

and the empty cavity eigenfunctions have the form

$$A_{pm}(\rho, \varphi, \eta) = B_m(\varphi)\, C_{pm}(\rho, \eta)\, \exp[i\theta_{pm}(\rho, \eta)] \tag{A.23}$$

where

$$B_m(\varphi) = \begin{cases} \dfrac{1}{\sqrt{2\pi}} & m = 0 \\ \dfrac{1}{\sqrt{\pi}} \sin m\varphi & m > 0 \\ \dfrac{1}{\sqrt{\pi}} \cos m\varphi & m > 0 \end{cases} \tag{A.24a}$$

$$C_{p,m}(\rho,\eta) = \frac{2}{v(\eta)} \left(\frac{2\rho^2}{v^2(\eta)}\right)^{m/2} \sqrt{\frac{p!}{(p+m)!}}\, L_p^m\left(\frac{2\rho^2}{v^2(\eta)}\right) \exp\left(-\frac{\rho^2}{v^2(\eta)}\right) \qquad (A.24b)$$

and

$$\theta_{pm}(\rho,\eta) = \frac{\rho^2}{u(\eta)} - (2p+m+1)\tan^{-1}\eta/\eta_1 \qquad (A.24c)$$

$p = 0,1,2,\ldots$ ; $m = 0,1,2,\ldots$.

The symbol $L_p^m$ indicates the associated Laguerre polynomial of order p and index m, and $v(\eta)$ and $u(\eta)$ are defined by Eqs. (A.8a) and (A.8b), respectively. The functions $A_{pm}$ form a complete orthonormal set and obey the orthogonality relation

$$\int_0^{2\pi} d\varphi \int_0^{\infty} d\rho\, \rho\, A_{pm}^{(i)\,*}(\rho,\varphi,\eta)\, A_{p'm'}^{(i')}(\rho,\varphi,\eta) = \delta_{pp'}\delta_{mm'}\delta_{ii'} \qquad (A.25)$$

The superscript i (i=1,2) distinguishes the solutions of type sin(mφ) from those of type cos(mφ), if $m \neq 0$ (for $m = 0$ the index i must be omitted). The eigenfrequencies of the ring resonator are given by

$$\omega_{n,p,m} = \frac{2\pi c}{\Lambda} n + \frac{2c}{\Lambda}(2p+m+1)\left[\tan^{-1}\frac{1-f}{2\eta_2} + \tan^{-1}\frac{f}{2\eta_1}\right] \qquad (A.26)$$

where

n, p, m = 0, 1, 2,...

For a resonator with a different mirror configuration from the one sketched in Fig. 2, Eq. (A.26) retains the same structure except for the geometry-dependent coefficient in the square brackets. A limiting case of our cavity configuration is $\rho_0 = f = 1/2$ in which $\eta_1 = \eta_2 = 1/4$ and the cavity frequencies are given by

$$\omega_{n,p,m} = \frac{\pi c}{\Lambda}\left[2(n+p) + m + 1\right] \qquad (A.27)$$

This situation is essentially identical to the standard confocal configuration.



## Appendix B - Recursion relation for the mode-mode coupling coefficients

We wish to derive a convenient recursion relation for the evaluation of the mode-mode coupling coefficients

$$\Gamma_{p,p',p''} = \int_0^{\infty} d\xi\, \xi\, \bar{A}_p\, \bar{A}_{p'}\, \bar{A}_{p''} \qquad (B.1)$$

where the modal functions are given by

$$\bar{A}_p(\xi) = 2\, L_p(2\xi^2)\exp(-\xi^2) \qquad (B.2)$$

With the change of variable $x = 2\xi^2$, Eq. (B.1) takes the explicit form

$$\Gamma_{p,p',p''} = 2\int_0^{\infty} dx \exp(-\tfrac{3}{2}x)\, L_p(x)\, L_{p'}(x)\, L_{p''}(x) \qquad (B.3)$$

Consider the two recursion relations

$$nL_n(x) = (2n-1-x)\, L_{n-1}(x) - (n-1)\, L_{n-2}(x), \quad n \geq 1 \qquad (B.4)$$

and

$$x\frac{dL_n(x)}{dx} = nL_n(x) - nL_{n-1}(x) \qquad (B.5)$$

With the help of Eq. (B.4) we can cast Eq. (B.3) in the form

$$\Gamma_{p,p',p''} = 2\int_0^{\infty} dx \exp(-\tfrac{3}{2}x)\, L_p\, L_{p'}\left(\frac{2p''-1}{p''}L_{p''-1} - \frac{x}{p''}L_{p''-1} - \frac{p''-1}{p''}L_{p''-2}\right) \qquad (B.6)$$

which yields at once

$$\Gamma_{p,p',p''} = \frac{2p''-1}{p''}\Gamma_{p,p',p''-1} - \frac{p''-1}{p''}\Gamma_{p,p',p''-2} - \frac{1}{p''}2\int_0^{\infty} dx \exp(-\tfrac{3}{2}x)\, x\, L_p\, L_{p'}\, L_{p''-1} \qquad (B.7)$$

The integral can be handled with an integration by parts according to the scheme

$$\int_0^\infty dx \exp(-\tfrac{3}{2}x)\, x\, L_p\, L_{p'}\, L_{p''-1} = \tfrac{2}{3}\int_0^\infty dx \exp(-\tfrac{3}{2}x)\left\{ x\frac{dL_p}{dx} L_{p'} L_{p''-1} + \right.$$

$$\left. + x\frac{dL_{p'}}{dx} L_p L_{p''-1} + x\frac{dL_{p''-1}}{dx} L_p L_{p'} + L_p L_{p'} L_{p''-1} \right\} \qquad (B.8)$$

and, with the help of Eq. (B.5), we finally arrive at the recursion relation

$$\Gamma_{p,p',p''} = -\frac{2p+2p'-4p''+3}{3p''}\Gamma_{p,p',p''-1} - \frac{1}{3}\frac{p''-1}{p''}\Gamma_{p,p',p''-2} + \frac{2}{3}\frac{p'}{p''}\Gamma_{p,p'-1,p''-1} +$$

$$+ \frac{2}{3}\frac{p}{p''}\Gamma_{p-1,p',p''-1}, \qquad p'' \geq 1 \qquad (B.9)$$

It is clear that if the coupling coefficients $\Gamma_{p,p',0}$ are known we can easily construct every other coefficient $\Gamma_{p,p',p''}$ with $p'' \geq 1$. We can derive a recursion relation for $\Gamma_{p,p',0}$ following the same procedure adopted above; we start from the definition

$$\Gamma_{p,p'} \equiv \Gamma_{p,p',0} = 2\int_0^\infty dx \exp(-\tfrac{3}{2}x)\, L_p\, L_{p'} \qquad (B.10)$$

we replace $L_{p'}(x)$ in terms of $L_{p'-1}$ and $L_{p'-2}$ [Eq. (B.4)] and integrate the remaining integral by parts with the help of Eq. (A.5). The result is the recursion relation

$$\Gamma_{p,p'} = -\frac{2p-4p'+3}{3p'}\Gamma_{p,p'-1} - \frac{1}{3}\frac{p'-1}{p'}\Gamma_{p,p'-2} + \frac{2}{3}\frac{p}{p'}\Gamma_{p-1,p'-1}, \qquad p' \geq 1 \qquad (B.11)$$

From standard tables of integrals we have

$$\Gamma_{p,0} = \frac{4}{3^{p+1}} \qquad (B.12)$$

Hence, the numerical strategy is clear: first we calculate $\Gamma_{p,0}$ ($p = 0, 1 \ldots p_{max}$) from Eq. (B.12), next we calculate $\Gamma_{p,p'\geq 1}$ from the recursion relation (B.11), and finally we calculate $\Gamma_{p,p',p''\geq 1}$ from Eq. (B.9). We have implemented this procedure and compared the results for selected coupling coefficients with those obtained from the direct numerical integration of Eq. (B.1). The comparison was very satisfactory [better than 4 digits even in single precision and for values of p as large as 30].



## Appendix C - Two mode stationary solution

Equations (3.4) are written in a frequency reference frame obtained by the usual mode pulling condition applied to the atomic and the p=0 mode frequencies. To properly analyze the steady state solutions we must shift the reference frame to the true unknown laser frequency via the transformation

$$\bar{\psi}_p^{st} = e^{i\xi t}\bar{\psi}_p = x_p + iy_p \qquad (C.1)$$

with a similar expression for the polarization variable. After setting the complex amplitudes for all modes but p=0 and p=1 equal to zero, we obtain four coupled algebraic equations for $x_0$, $\varepsilon$, $x_1$ and $y_1$

$$-x_0(1+2x_0^2+2x_0x_1+x_1^2) + \left[(a_1\frac{\varepsilon}{\kappa'} - \Delta')y_1 - g_1x_1\right](x_0^2+2x_0x_1+\frac{x_1}{2})$$

$$+x_0(\frac{\varepsilon}{\kappa'}+\Delta')(\varepsilon-\Delta'+x_0y_1+x_1y_1) - \left[(a_1-\frac{\varepsilon}{\kappa'}-\Delta')x_1+g_1y_1\right](x_0y_1+\frac{1}{2}x_1y_1)+2Cx_0=0 \qquad (C.2)$$

$$-x_0(\Delta'-\varepsilon+x_0y_1+x_1y_1)+x_0(\frac{\varepsilon}{\kappa'}+\Delta')(1+y_1^2)+\left[(a_1-\frac{\varepsilon}{\kappa'}-\Delta')y_1+g_1x_1\right](x_0y_1+\frac{1}{2}x_1y_1)$$

$$-\frac{y_1^2}{2}\left[(a_1-\frac{\varepsilon}{\kappa'}-\Delta')x_1+g_1y_1\right]=0 \qquad (C.3)$$

$$-x_0(x_0^2+2x_0x_1+\frac{1}{2}x_1^2)+x_0y_1(\frac{\varepsilon}{\kappa'}+\Delta')(x_0+\frac{1}{2}x_1)$$

$$+(1+x_0^2+x_0x_1+x_1^2)\left[(a_1-\frac{\varepsilon}{\kappa'}-\Delta')y_1-g_1x_1\right]-(\varepsilon-\Delta'+\frac{1}{2}x_0y_1+x_1y_1)\left[(a_1-\frac{\varepsilon}{\kappa'}-\Delta')x_1\right.$$

$$\left.+g_1y_1\right]+2Cx_1=0 \qquad (C.4)$$

$$-x_0y_1(x_0+\frac{1}{2}x_1)+\frac{1}{2}x_0y_1^2(\frac{\varepsilon}{\kappa'}+\Delta')+(\Delta'-\varepsilon+\frac{1}{2}x_0y_1+x_1y_1)\left[(a_1-\frac{\varepsilon}{\kappa'}-\Delta')y_1-g_1x_1\right]$$

$$-(1+y_1^2)\left[(a_1-\frac{\varepsilon}{\kappa'}-\Delta')x_1+g_1y_1\right]+2Cy_1=0 \qquad (C.5)$$

These equations are used in the text to evaluate the frequency shift ε due to the presence of the p=1 mode for pump values close to the first laser threshold.



## References


1. A.M. Turing, Phil. Trans. Roy. Soc. London B237, 37 (1952); H. Haken, Synergetics - An Introduction, Springer Verlag, Berlin, 1974; G. Nicolis and I. Prigogine, Self-organization in Non-equilibrium Systems, Wiley, New York, 1974.
2. E.N. Lorenz, J. Atm. Sci. 20, 130 (1963).
3. S. Grossmann and S. Thomae, Z. Natur. 32A, 1353 (1977); M.J. Feigenbaum, J. Stat. Phys. 19, 25 (1978); P. Coullet and C. Tresser, J. Phys. Coll. (Paris) C5, 39 (1978).
4. H.M. Gibbs, F.A. Hopf, D.L. Kaplan and R.L. Shoemaker, Phys. Rev. Lett. 46, 474 (1981)
5. F.T. Arecchi, R. Meucci, G.P. Puccioni and J.R. Tredicce, Phys. Rev. Lett. 49, 1217 (1982).
6. R.S. Gioggia and N.B. Abraham, Phys. Rev. Lett. 51, 650 (1983).
7. A.M. Albano, J. Abounadi, T.H. Chyba, C.E. Searle, S. Yong, R.S. Gioggia and N.B. Abraham, J. Opt. Soc. Am. B2, 47 (1985).
9. See for example, F. Heslot, B. Castaign and A. Libchaber, Phys. Rev. A36, 5870 (1987).
10. M. Le Berre, E. Ressayre and A. Tallet, Phys. Rev. A25, 1604 (1982).
11. D.W. McLaughlin, J.V. Moloney and A.C. Newell, Phys. Rev. Lett. 51, 75 (1983).
12. W.J. Firth, in Instabilities and Chaos in Quantum Optics II, edited by N.B. Abraham, F.T. Arecchi and L.A. Lugiato, Plenum Press , New York, 1988, p. 219.
13. L.A. Lugiato and R. Lefever, Phys. Rev. Lett. 58, 220 (1987); L.A. Lugiato and C. Oldano, Phys. Rev. A37, 3896 (1988).
14. J.V. Moloney and H.M. Gibbs, Phys. Rev. Lett. 58, 467 (1982).
15. J.V. Moloney, H. Adachihara, D.W. McLaughlin and A.C. Newell, in Chaos, Noise and Fractals, edited by E.R. Pike and L.A. Lugiato, Hilger, London, 1988, p. 137.
16. L.A. Lugiato, F. Prati, L.M. Narducci and G.-L. Oppo, Opt. Commun. 69, 387 (1989).
17. G. Grynberg, E. Le Bihan, P. Verkerk, P. Simoneau, J.R.R. Leite, D. Bloch, S. Le Boiteux and M. Ducloy, Opt. Commun. 67, 363 (1988).

18. G. Giusfredi, J.F. Valley, R. Pon, G. Khitrova, and H.M. Gibbs, J. Opt. Soc. Am. B5, 1181 (1988).

19. L.A. Lugiato, C. Oldano, and L.M. Narducci, J. Opt. Soc. Am. B5, 879 (1987).

20. L.A. Lugiato, G.-L. Oppo, M.A. Pernigo, J.R. Tredicce, L.M. Narducci and D.K. Bandy, Opt. Commun. 68, 63 (1988).

21. J.R. Tredicce, E.J. Quel, A.M. Ghazzawi, C. Green, M.A. Pernigo, L.M. Narducci and L.A. Lugiato, Phys. Rev. Lett. 62, 1274 (1989)

22. C. Tamm, Phys. Rev. A38, 5960 (1988).

23. L.A. Lugiato, L.M. Narducci, E.V. Eschenazi, D.K. Bandy, and N.B. Abraham, Phys. Rev. A32, 1563 (1985); L.M. Narducci, J.R. Tredicce, L.A. Lugiato, N.B. Abraham, and D.K. Bandy, Phys. Rev. A33, 1842 (1986).

24. L.A. Lugiato, F. Prati, L.M. Narducci, P. Ru, J.R. Tredicce and D.K. Bandy, Phys. Rev. A37, 3847 (1988).

25. A.F. Suchkov, Zh. Ek. T. Fiz 49, 1495 (1965) [Sov. Phys. JETP 22, 1026 (1966)].

26. R.G. Allakhverdyan, A.N. Oraevsky and A.F. Suchkov, Fiz. Tekh. Polup. 4, 341 (1970) [Sov. Phys. Semicond. 4, 227 (1970)].

27. V.E. Kuzin and A.F. Suchkov, Kvant Elek. 3, 52 (1972) [Sov. J. Quantum Electron. 2, 236 (1972)].

28. I.M. Belousova, G.N. Vinokurov, O.B. Danilov and N.N. Rozanov, Zh. Ek. T. Fiz. 57, 1146 (1967) [Sov. Phys. JETP 25, 761 (1967)].

29. P.W. Smith, Appl. Phys. Lett. 13, 235 (1968).

30. D.H. Auston, IEEE J. Quantum Electron. 5, 471 (1968).

31. P. Hollinger, C. Jung and H. Weber, Physica D (to be published).

32. P. Hollinger and C. Jung, J. Opt. Soc. Am. B2, 218 (1985); P. Hollinger, C. Jung and H. Weber, in Optical Instabilities, ed. by R.W. Boyd, M.G. Raymer and L.M. Narducci, Cambridge University Press, 1986, p. 260; see also M.L. Shih and P.W. Milonni, Opt. Comm. 49, 155 (1984).



33. C.O. Weiss and H. King, Opt. Commun 44, 59 (1982).

34. N.J. Halas, S.N. Liu and N.B. Abraham, Phys. Rev. A28, 2915 (1983).

35. D.J. Biswas and R.G. Harrison, Phys. Rev. A32, 3835 (1985).

36. P.Ru, L.M. Narducci, J.R. Tredicce, D.K. Bandy, and L.A. Lugiato, Opt. Commun. 63, 310 (1987).

37. See, for example, A. Yariv, Optical Electronics, 3rd edition, Holt, Rinehart and Winston (New York, 1985) p. 32.

38. P. Coullet, L. Gil, and J. Lega, Phys. Rev. Lett. 62, 1619 (1989).

## Figure Captions

Fig. 1 Schematic representation of a ring laser cavity with two spherical mirrors of radius of curvature $R_0$. The length of the ring is A, while the distance between the two curved reflectors is L. $\eta = 0$ indicates the origin of the longitudinal coordinate system and $\eta$ measures various longitudinal positions of relevance to our discussion, in units of A. The active medium is confined within the rectangular region of length $L_A$.

Fig. 2 Illustrating the significance of the two classes of transverse modes. The mode (n=N-1, p=3) is nearly degenerate with the reference mode (n=N, p=0). We have omitted the angular indices m for clarity of illustration.

Fig. 3 The shift of the laser carrier from the reference frequency in a range of parameters where the competition between the p=0 and p=1 modes leads to stationary solutions. (a) Plot of the curve (3.11) obtained via perturbative expansion of the steady state equations, (b) numerical integration of Eqs. (3.4) for $\kappa'$=1.0. The other parameters are fixed to the values reported in the text.

Fig. 4 Scan of the total flux as a function of the modal spacing $a_1$ for (a) $\kappa'$=1.0, (b) $\kappa'$ =0.3. The other parameters are selected as stated in the text. For each value of $a_1$, we plot the maximum and minimum excursion of the oscillations after the transients have died out.

Fig. 5 Time evolution of the first three modal amplitudes during the scan of Fig. 4 for $\kappa'$=1.0 (curves a1, a2, a3) and $\kappa'$ =0.3 (curves b1, b2, and b3). The other parameters are selected as stated in the text.

Fig. 6 Spatio-temporal evolution of the modulus of the output field for $\kappa'$=1.0, (a) $a_1$=0.34, (b) $a_1$=0.32, and (c) $a_1$=0.25. The other parameters are selected as stated in the text.

Fig. 7 Radial dependence of the correlation function $C_{max}(0,\rho)$ for the spatio-temporal evolutions of Fig. 6.

Fig. 8 Schematic representation of the empty resonator. The meaning of the symbols is the same as in Fig. 1

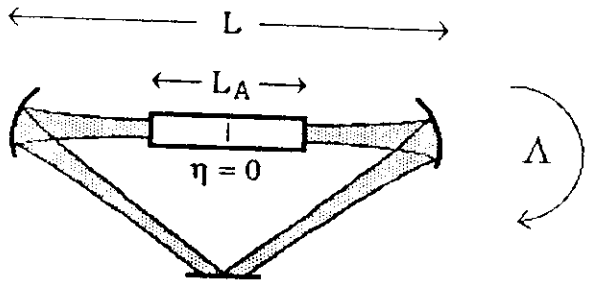


Fig. 1

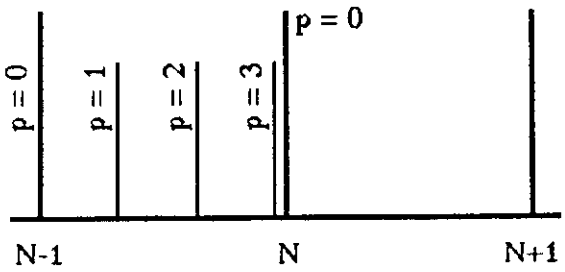


Fig. 2

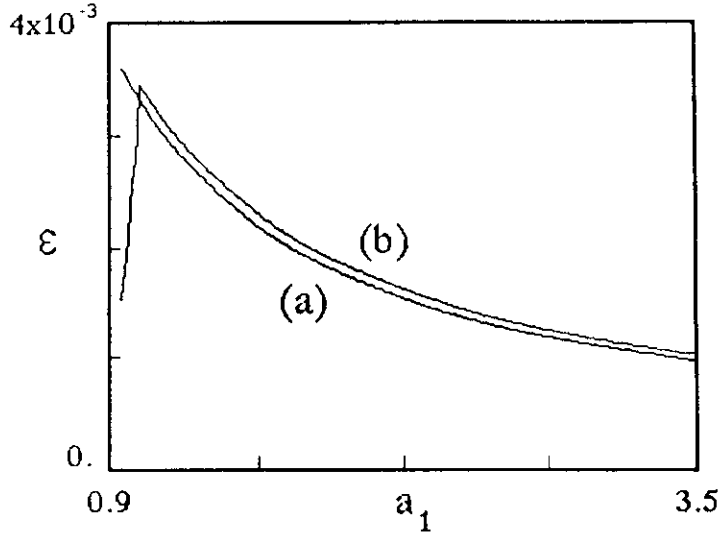


Fig. 3

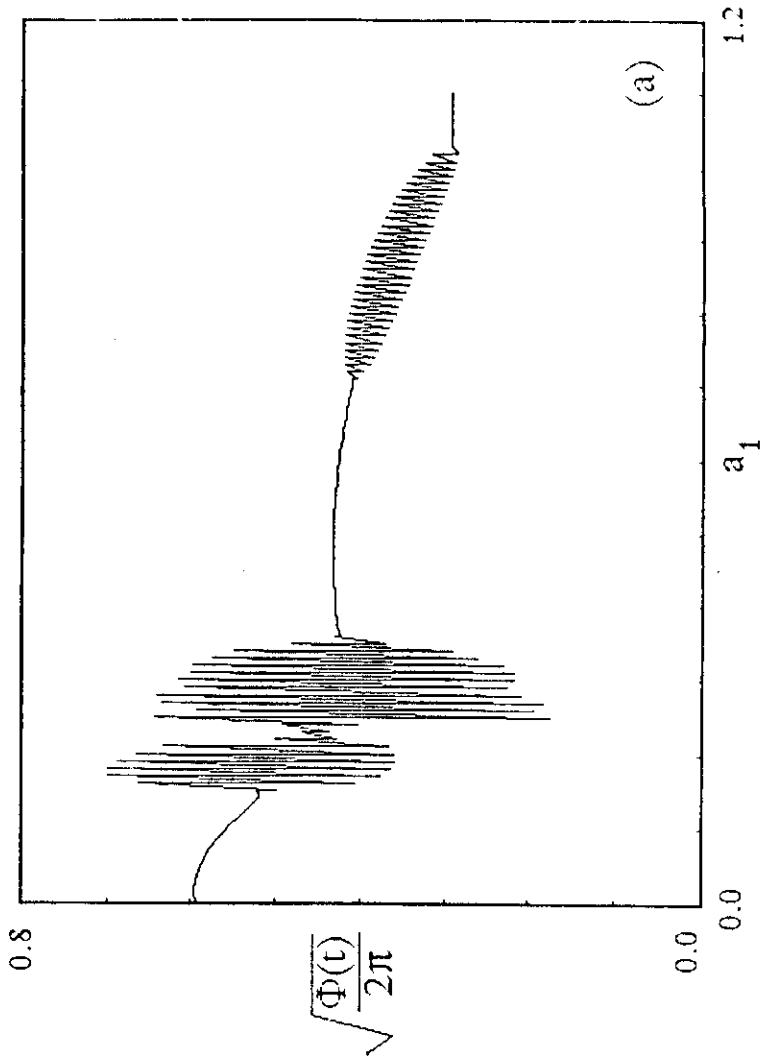
(a)
0.8
0.0
1.2
0.0
$a_1$
$\sqrt{\frac{\Phi(t)}{2\pi}}$

Fig. 4a

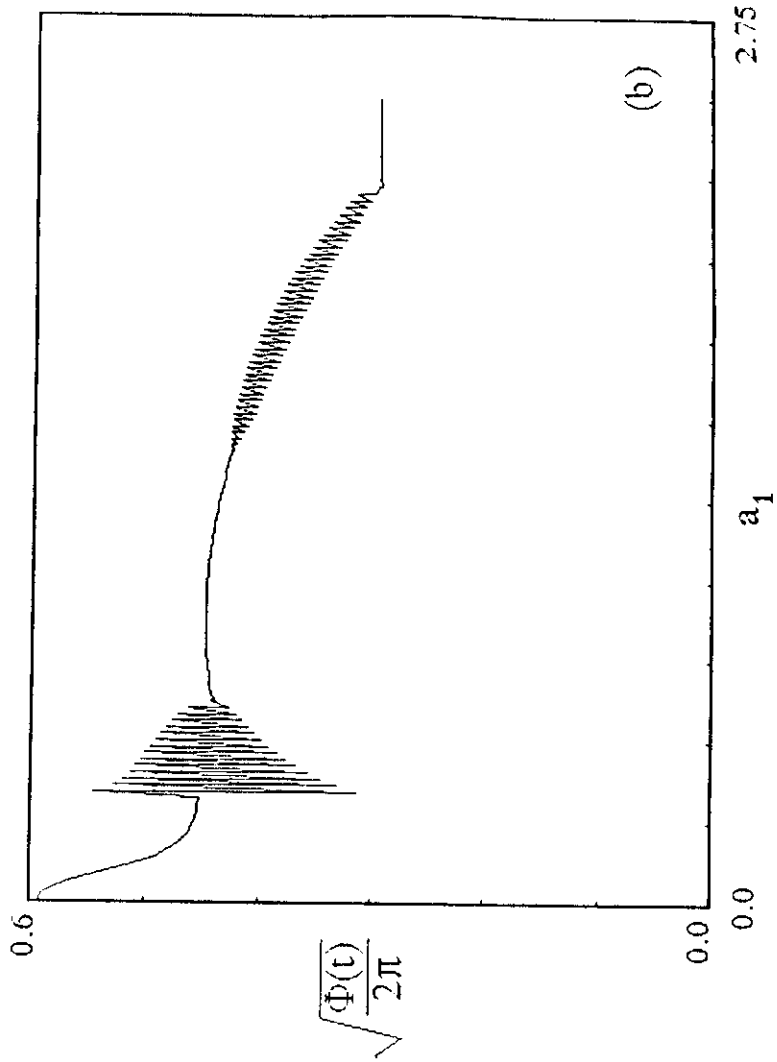
(b)
0.6
0.0
2.75
0.0
$a_1$
$\sqrt{\frac{\Phi(t)}{2\pi}}$

Fig. 4b

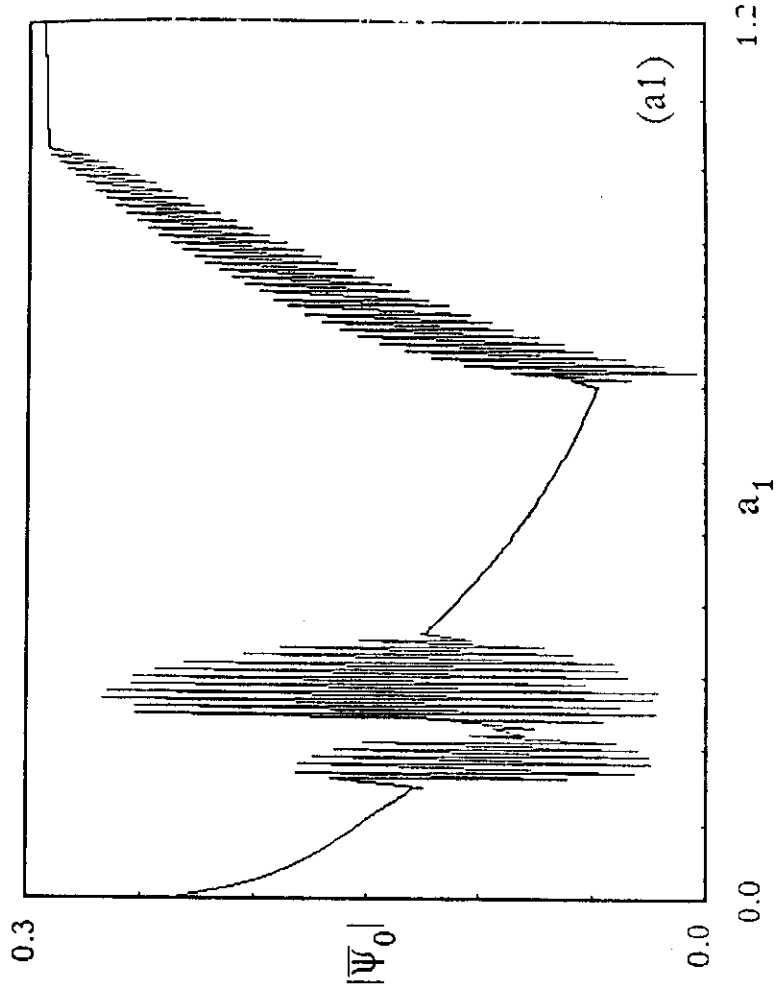


Fig. 5 (a1)

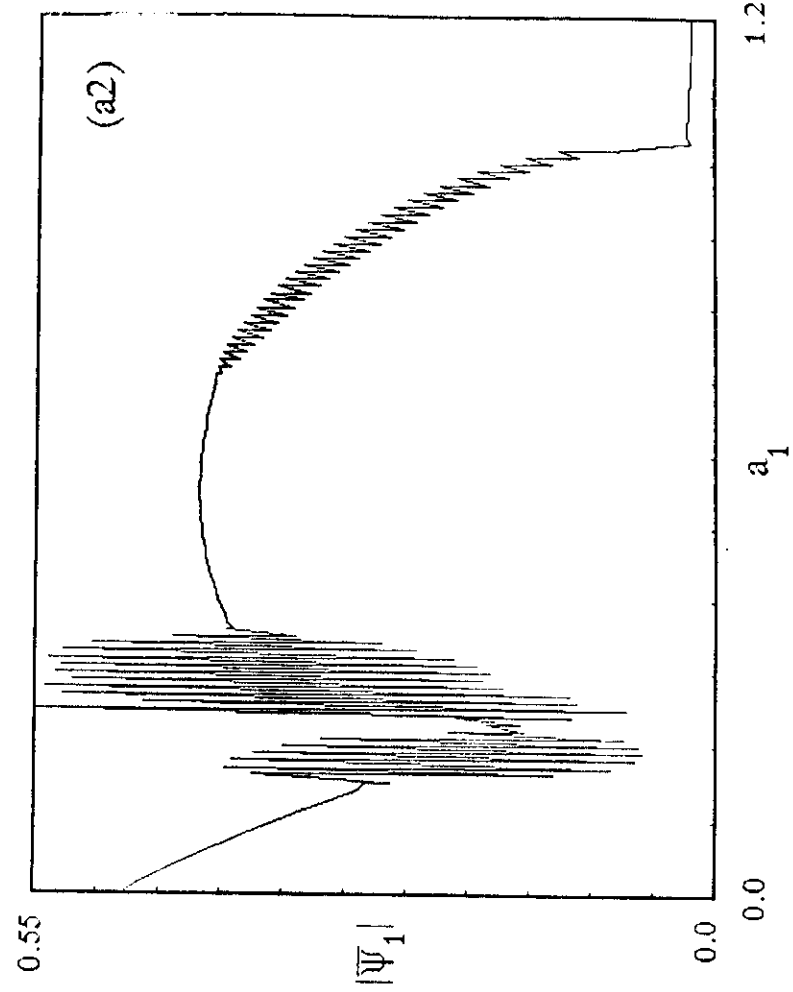


Fig. 5 (a2)

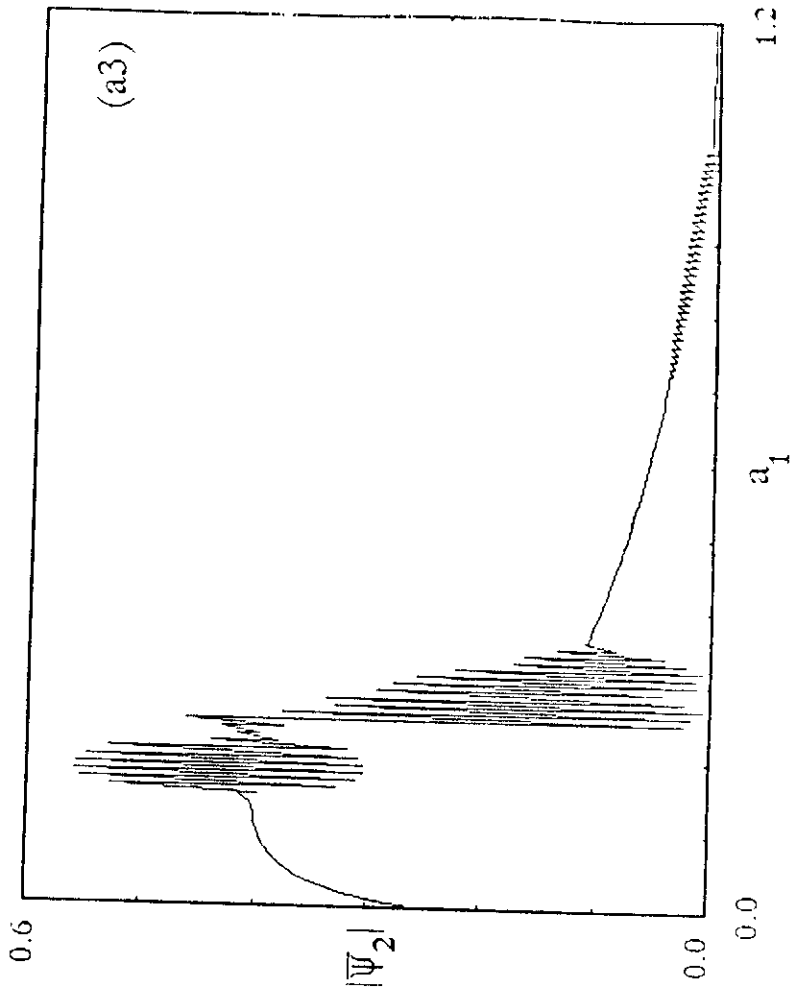


Fig. 5 (a3)

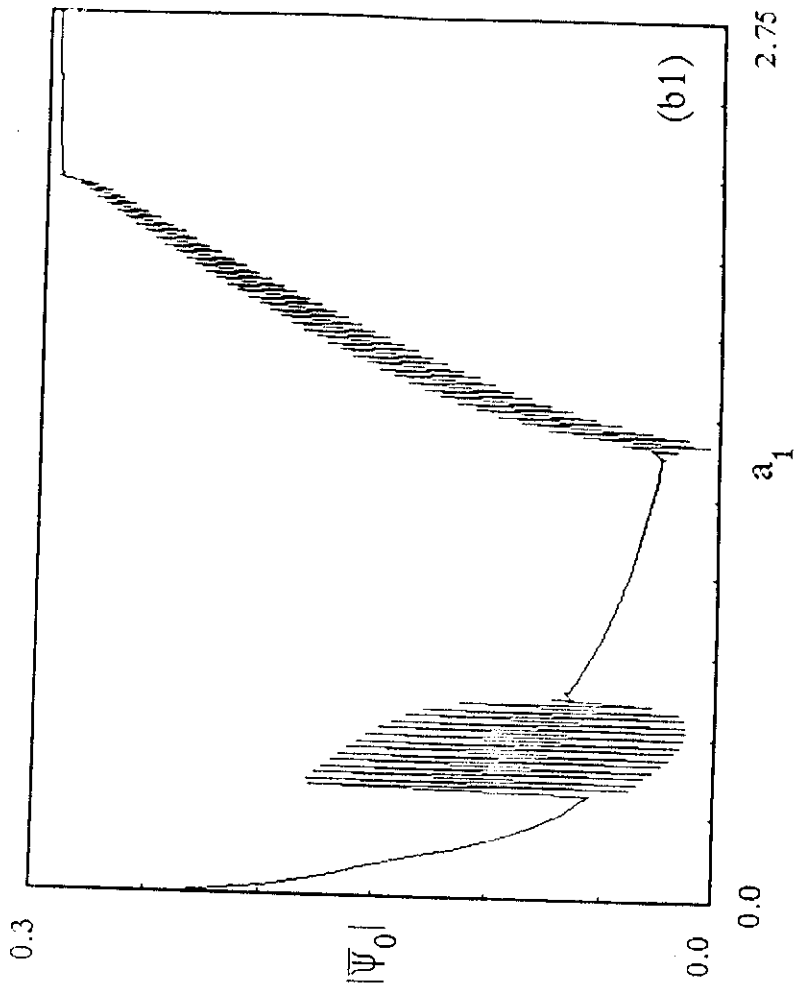


Fig. 5 (b1)

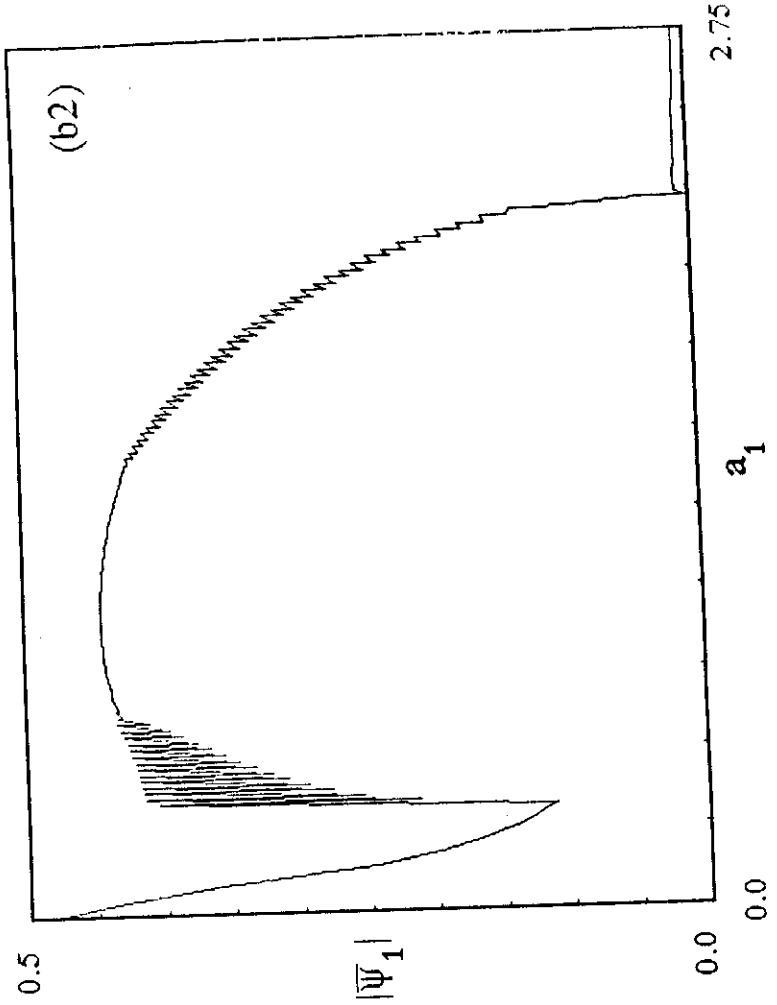


Fig. 5 (b2)

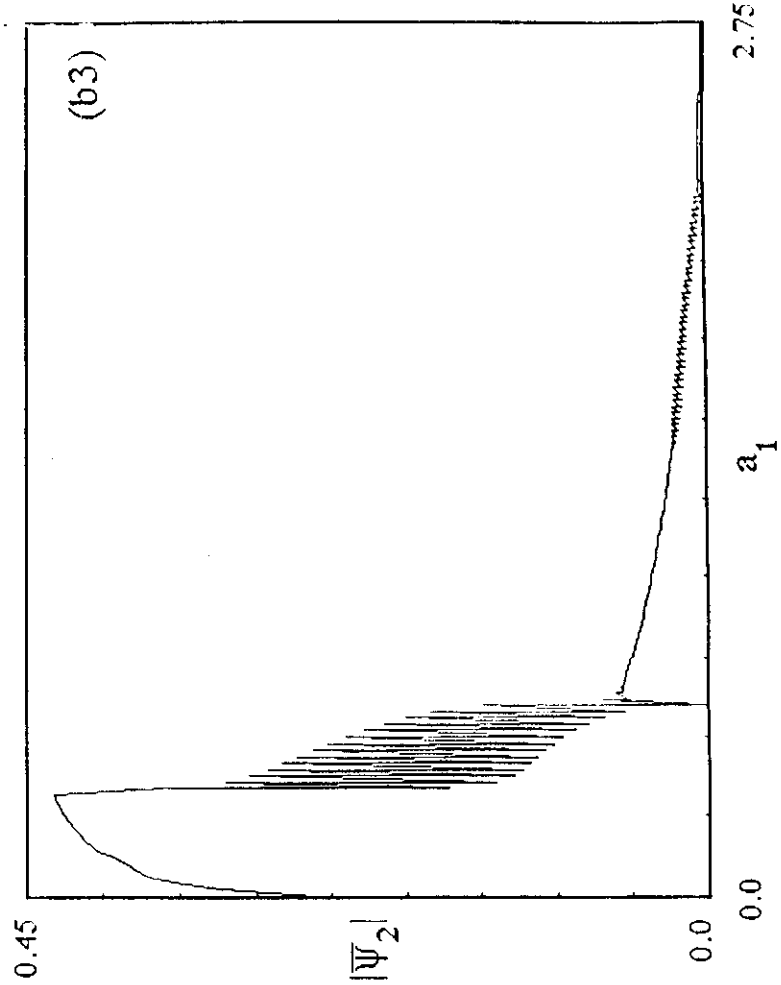


Fig. 5 (b3)

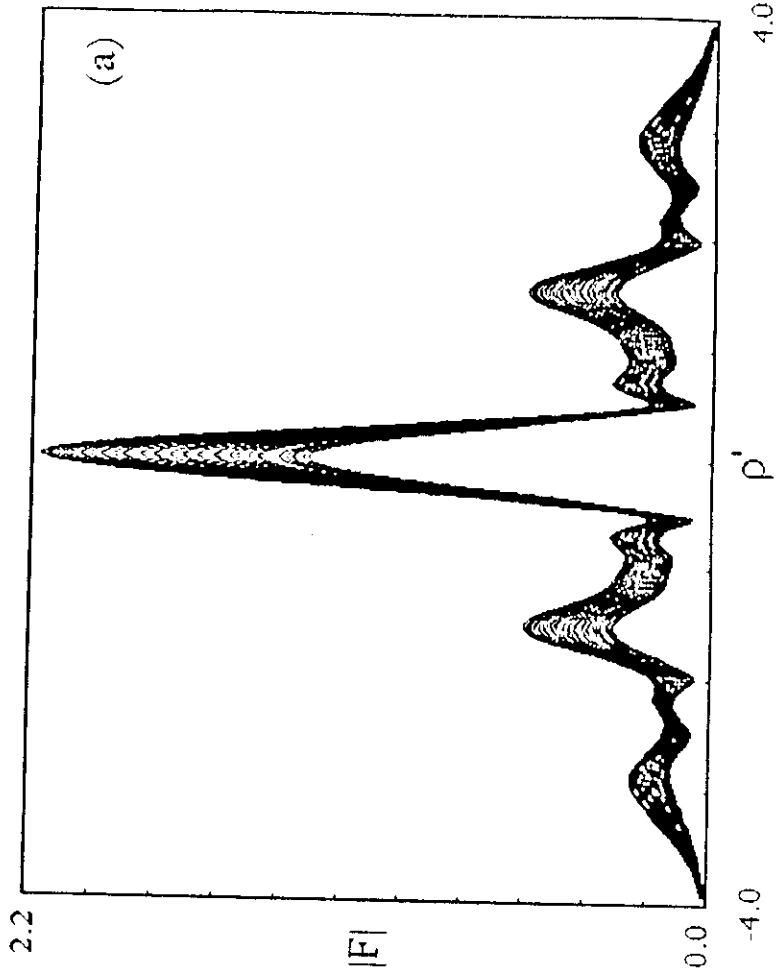


Fig. 6a

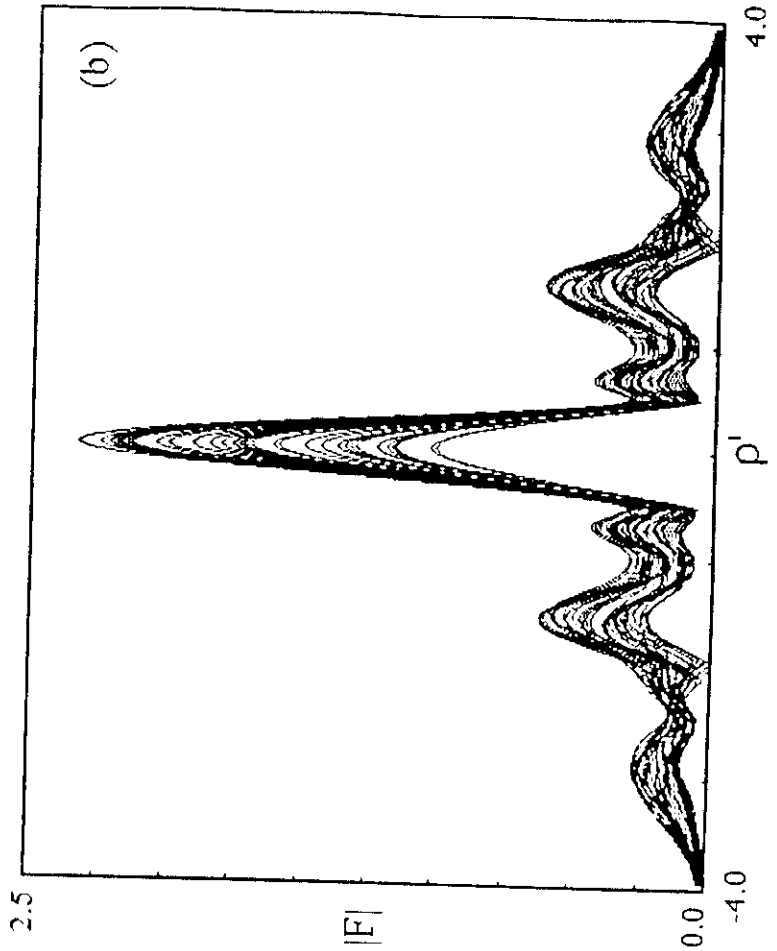


Fig. 6b

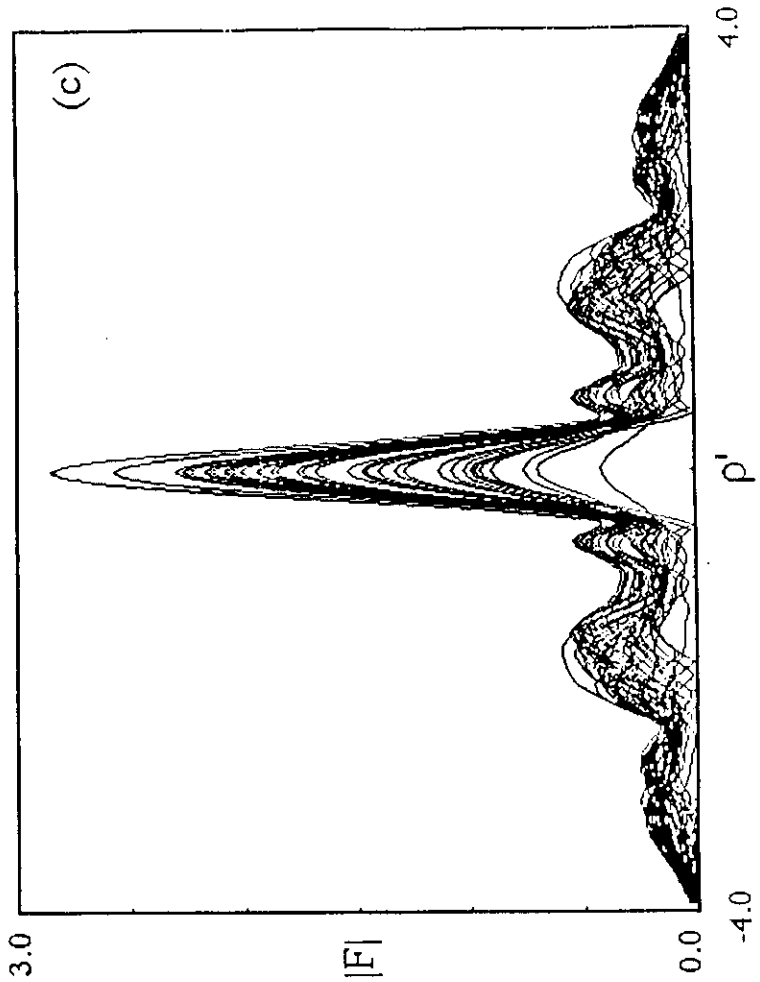


Fig. 6c

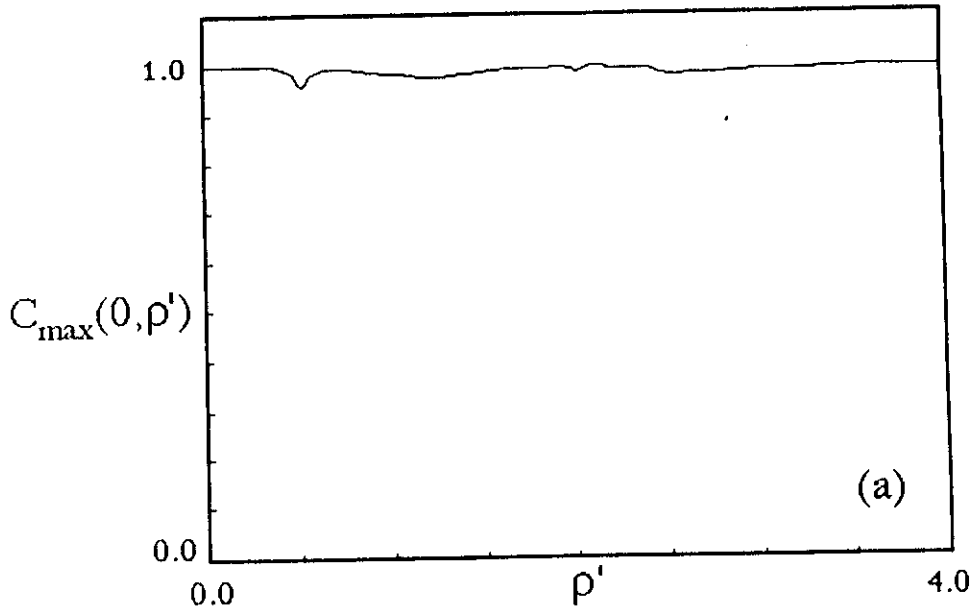


Fig. 7a

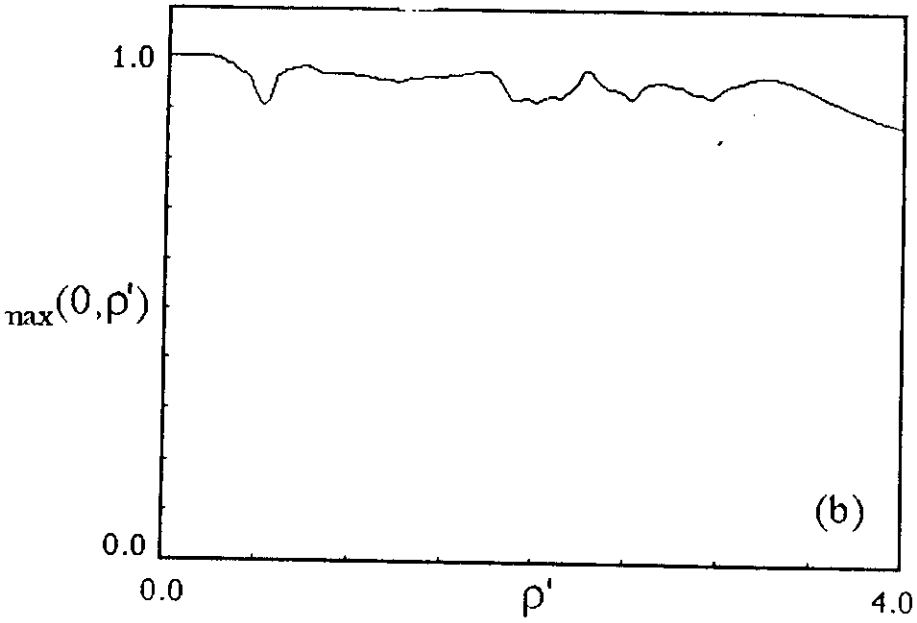


Fig. 7b

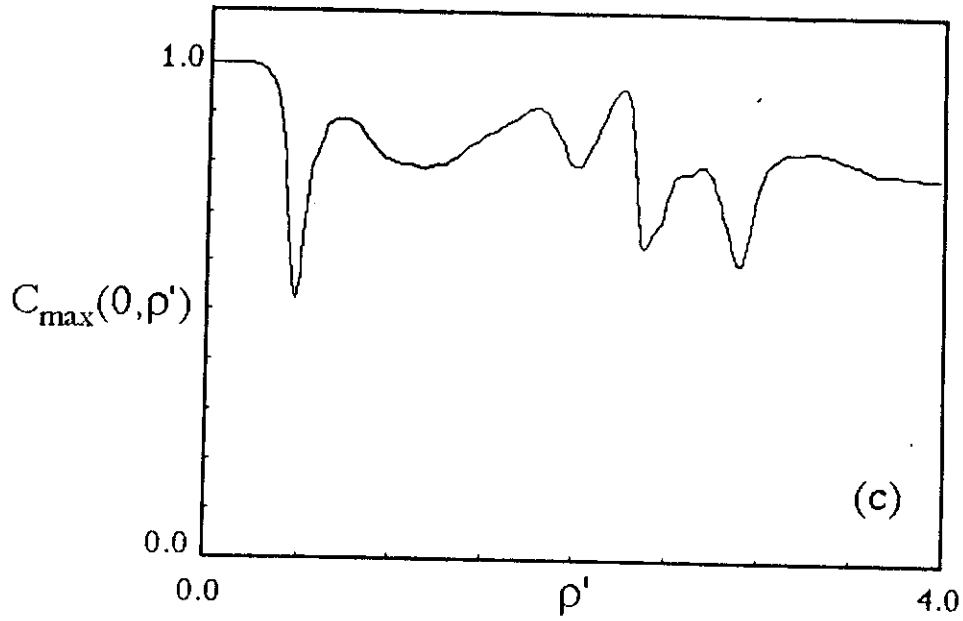


Fig. 7c

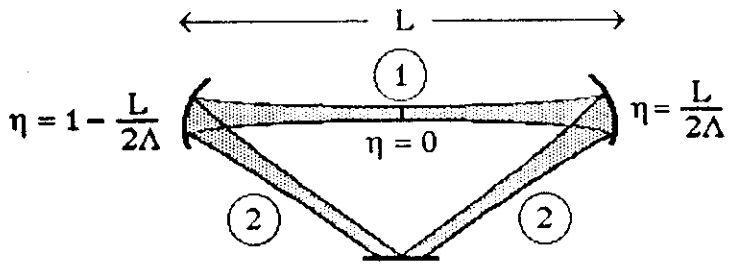


Fig. 8